University of Southern Queensland

Faculty of Health, Engineering & Sciences

Dual-Camera Infrared Guidance for Computed Tomography Biopsy Procedures

A thesis submitted by

Bruce Shar

for the award of

Doctor of Philosophy

2017

Abstract

A CT-guided biopsy is a specialised surgical procedure whereby a needle is used to withdraw tissue or fluid specimen from a lesion of interest. The needle is guided while being viewed by a clinician on a computed tomography (CT) scan. CT guided biopsies invariably expose patients and operators to high dosage of radiation and are lengthy procedures where the lack of spatial referencing while guiding the needle along the required entry path are some of the difficulties currently encountered. This research focuses on addressing two of the challenges clinicians currently face when performing CT-guided biopsy procedures.

The first challenge is the lack of spatial referencing during a biopsy procedure, with the requirement for improved accuracy and reduction in the number of repeated scans. In order to achieve this an infrared navigation system was designed and implemented where an existing approach was subsequently extended to help guide the clinician in advancing the biopsy needle. This extended algorithm computed a scaled estimate of the needle endpoint and assists with navigating the biopsy needle through a dedicated and custom built graphical user interface.

The second challenge was to design and implement a training environment where clinicians could practice different entry angles and scenarios. A prototype training module was designed and built to provide simulated biopsy procedures in order to help increase spatial referencing. Various experiments and different scenarios were designed and tested to demonstrate the correctness of the algorithm and provide real-life simulated scenarios where the operators had a chance to practice different entry angles and familiarise themselves with the equipment. A comprehensive survey was also undertaken to investigate the advantages and disadvantages of the system.

Associated Publications

The following publications were produced during the period of candidature:

Shar, Bruce and Leis, John, "Towards three-dimensional fusion of infrared guidance measurements for biopsy procedures: some preliminary results and design considerations.", *Signal Processing and Communication Systems (ICSPCS), 4th International Conference on. IEEE, 13 - 15 Dec 2010, Gold Coast, Australia.*

Shar, Bruce and Leis, John, "Infrared camera imaging algorithm to augment CT-assisted biopsy procedures", *6th International Conference on Signal Processing and Communication Systems (ICSPCS 2012), 12-14 Dec 2012, Gold Coast, Australia.*

Shar, Bruce and Leis, John, "Infrared Navigation System for CT Guided Procedures", *Research forum, School of Medicine, PA Hospital, May 2014, Brisbane, Australia .*

Shar, Bruce and Leis, John, "2D Mapping of CT Biopsy Fiducial Points using Two Infrared Cameras and DICOM Images", *8th International Conference on Signal Processing and Communication Systems, 15-17 Dec 2014, Gold Coast, Australia .*

Shar, Bruce and Leis, John, "Real-Time 3D Mapping of Biopsy Fiducial Points using Two Infrared Cameras", *The 22nd International Conference on Mechatronics and Machine Vision in Practice (M2VIP), 8-9 Dec 2015, Toowoomba, Australia.*

Shar, Bruce and Leis, John, "Mapping of Computer Tomography Biopsy Procedure Points using Two Infrared Cameras and DICOM Images", *Submitted to: Journal of Medical & Biological Engineering & Computing, Jan 2017.*

Certification of Thesis

This thesis is entirely the work of Bruce Shar except where otherwise acknowledged. The work is original and has not previously been submitted for any other award, except where acknowledged.

Student and supervisors' signatures of endorsement are held at USQ.

Acknowledgments

I would like to express my sincerest gratitude to my supervisor, Dr. John Leis, for the support and encouragement he has provided me throughout the years as his student. Thank you for being such an approachable and supportive mentor.

I also acknowledge the assistance of my colleague and dear friend Dr Eric Sclavos, Consultant Radiologist, Nuclear Medicine Physician and Founding Executive Partner of Qscan Radiology Clinics for always believing in me.

Bruce Shar

Contents

List of Figures

List of Tables

Acronyms & Abbreviations

ALARA	As Low As Reasonably Achievable
CT	Computed Tomography
CTDI	CT Dose Index
DICOM	Digital Imaging and Communications in Medicine
DLP	Dose Length Product
EM	Electromagnetic
FOV	Field of View
Gy	Grey Unit
kVp	Kilovolt Peak
LAR	Lifetime Attribution Risk
LED	Light Emitting Diode
LD	Low Dose
mAs	Milliamp Seconds
MDCT	Multi-detector technology
MRI	Magnetic Resonance Imaging
mSv	Millisievert
NIR	Near Infrared
OECD	Organisation for Economic Co-operation and Development
PACS	Picture Archiving and Communication System
PET	Positron Emission Tomography
PLB	Percutaneous Lung Biopsy
US	Ultra Sound

Chapter 1

Introduction and Research Aims

Computed Tomography (CT) is an imaging technique extensively used for diagnostic purposes. It offers comprehensive assessment of anatomical structures and functions. CT studies provide a cross-sectional picture of internal organs and tissues as depicted in Figure 1.1. CT guided biopsy procedures are used to assist a clinician withdraw tissue or fluid specimen from a lesion of interest inside a patient. The needle is guided through the patient while being viewed by the clinician in a stepwise fashion on multiple CT scans (Hsieh 2009). Through the use of CT scanner technology, clinicians are able to accurately place a biopsy needle into a lesion of interest with a high degree of success and with a low risk to the patient. This approach has significantly improved the way in which medical diagnoses are made. For example, exploratory laparotomies for suspected tumors have decreased significantly due to the increasing use of CT guided biopsies of suspicious masses (Gruber-Rouh et al. 2015*a*).

In parallel, the advances of computing science in medicine has enabled the integration of technologies such as navigation systems and devices with image-based guidance, which has provided ways to improve accuracy and efficiency and has helped reduce the amount of radiation exposure to both patients and operators. The integration of computer assistive devices with image-based guidance has the potential to improve accuracy and efficiency and as a result reduce patients trauma and radiation dose (Busse et al. 2007) and as such it is the main focus of this research.

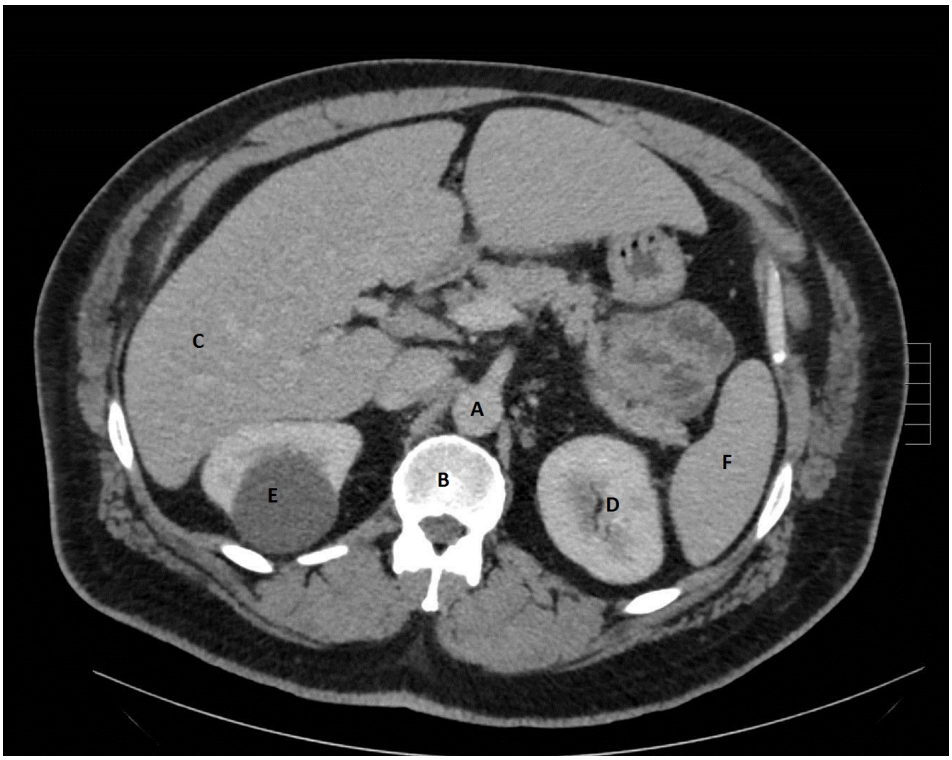

Figure 1.1: A typical medical CT image A: Aorta, B: Spine, C: Liver, D: Kidney, E: Cyst, F: Spleen. Image Courtesy of the Princess Alexandra Hospital, Radiology Department.

This thesis examines infrared technology and potential applications in the field of Radiology including fine needle aspirations which are performed by passing a thin needle through the skin to sample fluid or tissue from a cyst or solid mass of the lung, liver, nodes or bones (Na et al. 2012). Other Radiology specific procedures which an infrared navigation system could be applied to include therapeutic injections of joints, nerve roots and epidural, radiofrequency ablation and drain placements (Seeram 2009).

During a biopsy, the needle is placed in the patient's body and all necessary adjustments are done to align the needle perfectly with the predicted target prior to piercing the skin. The anticipated path of the needle is traced on a series of CT scans extrapolating the needle towards the lesion (Yu et al. 2009). Smaller sub-pleural lesions (lesions situated between the pleura and the body wall) usually require CT guidance. Small sub-pleural lesions are also difficult to biopsy because a short needle length inside the body is unstable and can be easily dislodged during respiratory motion (Lal et al. 2012). There is a clear demand for a natural and intuitive system (Peters 2001) which could play a major role in the guidance of surgical procedures as highlighted in the survey (Appendix G).

1.1 The Context of the Research

Radiologists at the Princess Alexandra Hospital (PA Hospital), Brisbane perform more than 500 CT biopsies per year. This number of biopsy sessions is consistent with a large Australian metropolitan teaching hospital and is an increasing trend as depicted in Table 1.1. Each CT biopsy procedure currently takes about an hour and involves at least one radiologist, three Radiographers, one nurse and one medical imaging assistance. It exposes the patient and the operators to radiation and it is a extremely time consuming, expensive and labor intensive procedure.

Table 1.1: CT Biopsy Numbers at PA Hospital

Number of CT Biopsy Procedures at the Princess Alexandra Hospital						
Year	2010	2011	2012	2013	2014	2015
CT Biopsies	173	203	204	211	380	563

CT guided biopsy procedures are performed by initially positioning the needle at a rough estimation of the desired angle, and then slowly advancing the needle into the patient's body, taking numerous CT scans along the way to determine the actual position of the needle, altering its trajectory as needed. This trial and error technique has major disadvantages which will be discussed in Chapter 2. The potential to reduce radiation to patients and operators, reduced the time and costs that the procedure takes and reduced training requirements are all very important and as such are the main focus of this research. With these aims, two main objectives were identified.

The first objective was the design and implementation of a navigation system which included both software and hardware components. The software components include localisation and tracking algorithms and graphical user interface. The hardware components are comprised of infrared cameras, emitters, reflectors and a biopsy needle. The second objective was to use the navigation system for the purposes of training where a trainee clinician could practice navigating a biopsy needle towards a target. Various CT biopsy scenarios were constructed with the help of senior clinicians and then tested using freehand method versus guidance method which will be further discussed in Chapter 4.

1.2 Research Motivation

Despite the clear evidence that CT scanning provides valuable information for diagnosis and patient management, there are still risks associated with them. The main concern is the potential risk of radiation-induced malignancy (Beir 2006). The primary motivation behind this research is to identify these risks and to work towards decreasing them.

According to the radiation protection guideline As Low As Reasonably Achievable (ALARA), any method that can be implemented which reduces or eliminate radiation dose must be made available for radiographic procedures (Slovis 2003). ALARA is not only a sound safety principle, it is a regulatory requirement for all radiation procedures (Teeuwisse et al. 2001). Reduction in radiation dose is critical, particularly in light of the continued increase in the number of CT examinations performed annually (Yu et al. 2009). Therefore if infrared navigation is indeed a viable method that contributes to radiation dose reduction, then it would become a requirement for biopsy procedures.

In a situation where the lesion of interest being biopsied is difficult to safely access, radiologists use a double angle method which involves angling the needle in two planes, left/right and up/down. In order to accurately hit the lesion of interest, the angles need to be very precise. At present to ensure precise positioning, the CT gantry is tilted to the required angle. The radiologist then inserts the needle into the patient, and uses the gantry laser lights as a guide for the up/down angle as required (Webb et al. 2014*a*). As a result of the size and engineering challenges, newer CT scanners are unable to tilt the gantry (Arnolli et al. 2015). Consequently, there is a developing need for an alternative method of performing the double angled biopsies under CT-guidance.

Several approaches to CT-guided biopsy procedures have been investigated and will be discussed in Chapter 3. There is no consensus regarding an optimal biopsy navigation system. The reason lies in the complexity of such a system, whose performance depends equally and critically on several components, namely the biopsy tracking performance and the visualisation capabilities combined with control of the instrument positioning mechanism. In order to achieve accurate targeting, optimisation of these components is essential and this need provides the motivation for this research.

1.3 Contributions of this Research

This research provides clinicians with a simple and easy to use method for biopsy needle guidance. It assists the operator by addressing the lack of spatial referencing. This was highlighted as one of the main advantages of this system in the survey (Appendix G) completed by clinicians who used the system. The results of the survey are discussed in chapter 6 where they advantages and disadvantages of the system are reviewed. In the survey majority of the operators considered the system useful for addressing the lack of spatial referencing during a biopsy procedure. It does not try to control any instruments nor does it attempt to identify patient physiology. It demonstrates that both patients undergoing and clinicians performing a biopsy procedure can benefit from an infrared navigation system which is integrated into a CT scanner.

A method described by Zhang (2000) was modified to employ data from multiple cameras, extending it to two IR cameras. Furthermore, the use of a training module where trainee radiologists would practice biopsy scenarios was also investigated and a detailed survey conducted where the operators have identified the advantages and disadvantages of the system and some of the main difficulties with CT guided biopsy procedures identified and potential solutions discussed. In section 6.2 using the top box method, the results are analysed and show a positive indication.

The work completed in this research proves the concept and the extended algorithm. The algorithm has been demonstrated to achieve higher accuracy in a realistic setting. If the proposed infrared navigation system is further integrated into a CT scanner for use with real patient biopsy procedures, some of the benefits would include:

- Clinicians will not need to conduct repeated X-rays to correct the trajectory of the needle.
- The system would save time, money and most importantly reduce radiation to both patient and operators.
- Clinicians will be able to improve their special referencing and biopsy skills by practicing biopsy scenarios.

1.4 Research Outline

The key challenges in achieving efficient and accurate navigation of the biopsy needle are fast and robust tracking, accurate registration and reliable and effective visualisation of both needle and target. The significance of these issues is outlined here and the solutions presented in this thesis are introduced. Key aspects in developing the navigation and training systems are also presented with the aim to develop an optimised navigation system suitable for assisting with CT-guided biopsy procedures which includes accurate tracking of the biopsy needle, real-time visual feedback of the location of the needle in relation to the target, increased spatial reference of the operator and increased confidence to perform the procedure. The specific objectives were as follows:

1. Development and validation of a method to navigate a biopsy needle by receiving feedback of the position of the needle in relation to the identified target.
2. Development and validation of the infrared navigation system software. The localisation and tracking algorithms and graphical user interface.
3. Development and validation of the infrared navigation system hardware. This included the markers for instrument tracking, infrared cameras, emitter and reflectors.
4. Development and validation of a training module where operators can practice biopsy scenarios in a test environment.
5. Surveys and analysis conducted by radiologists who use the training module to practice biopsy scenarios.

These aims and objectives have been verified and demonstrated using experimental results and survey completed by the system operators. Ethical clearance was granted for the use of the CT scanner and equipment in the radiology department of the Princess Alexandra Hospital in Brisbane (Appendix F). This was a major challenge because CT scanners are extremely valuable and must only be operated by health professionals trained in CT protocols and procedures. The hospital recognised the importance of what this research is trying to achieve and as such not only granted the ethical clearance of images, but also the repeated use of the CT scanners and health professionals' valuable time to complete this research.

1.5 Structure of the Thesis

This thesis encompasses contextual assessment, software and hardware integration, and testing in a clinical scenario. The chapters are organised as follows:

Chapter 2 presents background theory and information on CT imaging, including the hardware and software components of CT scanners.

Chapter 3 reviews the current literature, covering previous work in navigation systems and biopsy procedures and target imaging, with a focus on CT-guided biopsy procedures.

Chapter 4 hardware & software used to conduct the experiments and the methods used for image based guidance of the biopsy needle and setup of the training module.

Chapter 5 develops algorithms in order to provide information display and analysis, proposed future developments, and a list and clinical assessment of the system.

Chapter 6 presents the clinical performance evaluation where a comprehensive survey completed by clinicians who have used the system is analysed.

Chapter 7 concludes the thesis with a review of the work done, proposed future developments and a list of the outcomes of the research.

Appendix A results - Freehand Method v Infrared Guidance.

Appendix B results - Infrared to DICOM.

Appendix C 2D to 3D Transformation Results.

Appendix D training Module.

Appendix E connect client to drivers, read and run the program.

Appendix F ethical clearance.

Appendix G radiologist survey questions.

Appendix H radiologist survey results.

Chapter 2

Research Context and Clinical Background

This chapter presents background theory and information on CT imaging including CT guided biopsy procedures, biopsy needles, radiation dose, DICOM and CT scanner technology.

2.1 Computed Tomography

Computed tomography (CT) is a diagnostic imaging examination used to create detailed images of internal organs, soft tissue, bones and blood vessels (Lal et al. 2012). Since its introduction in 1973, CT has established itself as one of the primary diagnostic imaging modalities (Beckmann 2014). As depicted in Figure 2.1, CT technology has advanced considerably from the time of its introduction. It continued to advance and in the late 1980s helical scanning techniques were introduced (Webb et al. 2014*b*) which enabled movement in a helical pattern thus increasing the image resolution significantly. Soon after, with the development of multidetector-row technology in the late 1990s (McCollough et al. 2009), faster scanning and thinner collimation allowed routine scans to be performed faster with higher z-axis resolution. Today, the quality, number and impact of clinical applications of CT continues to grow.

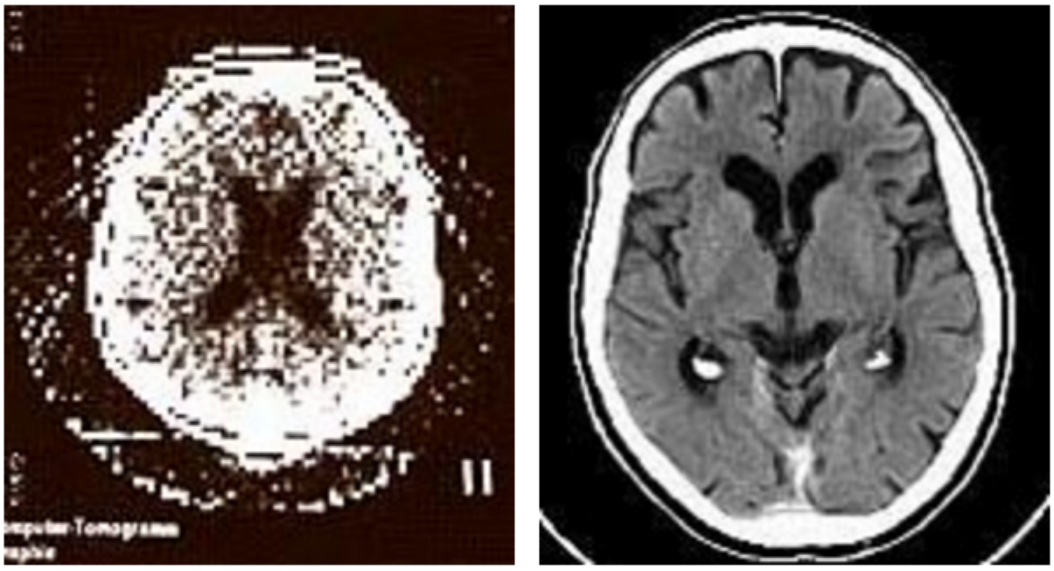

Figure 2.1: Left: Circa 1975, early days of the CT scanning. Right: Current CT imaging of the brain. The two images demonstrate how much image quality has progressed over the last 4 decades (*Siemens Circa 1975* n.d.).

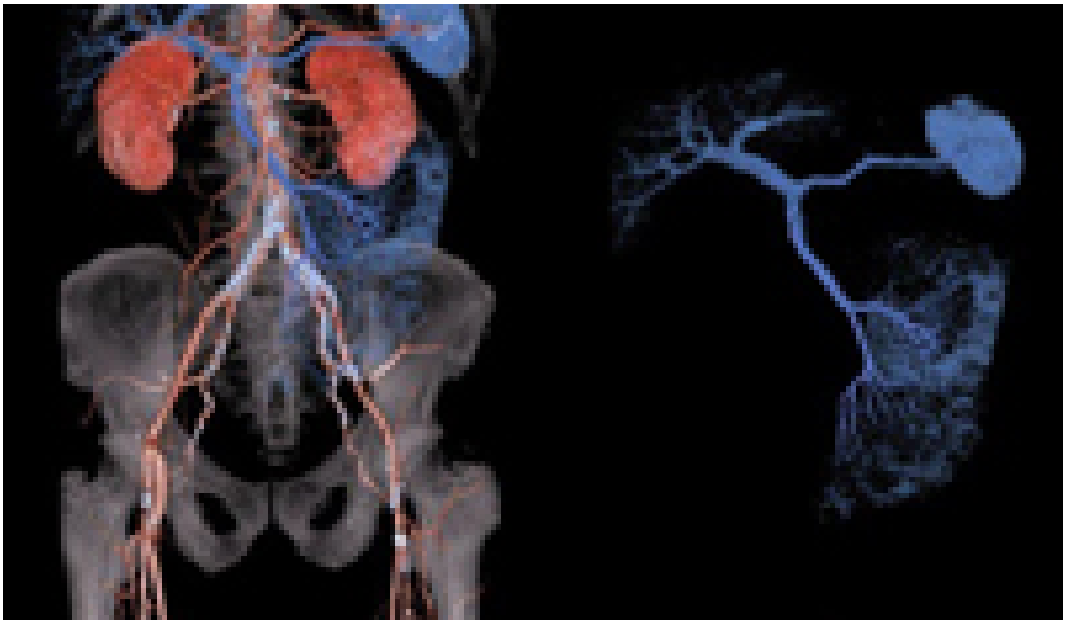

Figure 2.2: Radiology rendering software used to generate a 3D CT study of a de-identified patient.

Multiple plane reformatting can be applied to the cross-sectional images generated during a CT scan, and radiological software can even generate three-dimensional images as demonstrated in Figure 2.2. These images are put together in series and combined to make up medical imaging studies which can be displayed on a computer monitor, printed

on hard copy film or transferred to electronic media (Herman 2009).

CT scanning is one of the most effective methods for detecting different types of cancers. CT images enable clinicians to confirm the presence, location and size of a tumour. CT scans are fast, painless, noninvasive and accurate. In emergency cases, CT scans quickly help emergency clinicians identify internal injuries and bleeding allowing them fast response which is often critical to the patient's survival. Using fast scanning speed and isotropic (uniformity in all orientations) spatial resolution at 0.3 to 0.4 mm (Taguchi et al. 2000), CT enables clinicians to diagnose injuries and disease much quicker, safer and more accurately than other more invasive imaging techniques which require more recovery time for the patients (Yu et al. 2009). CT imaging also plays a major part in the staging, treatment planning and follow up of cancer cases as a detailed comparison can be performed when new CT scans are compared to older CT scans. The advantages of using CT scanning is recognised in medicine and as such its use is now pervasive in modern medical practice. It is estimated that 110 CT examinations per 1000 population were performed in 2013 in Australia Figure 2.3 which is up 5 percent since 2012 (*OECD Health Data* 2016).

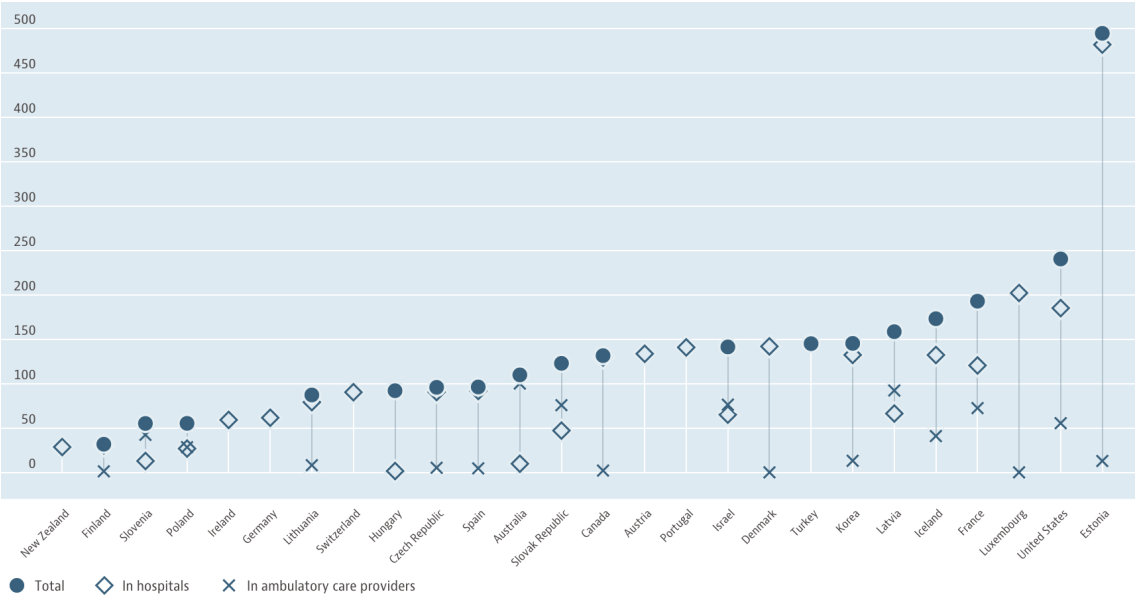

Figure 2.3: CT Scans per 1000 inhabitants OECD Health Data.

The significant benefits to health-care afforded by CT have ensured continuing steady growth in both scanner technology and clinical application (Golding 2002). CT practice continues to evolve with new technologies and at the same time there is increasing atten-

tion to optimisation of patient protection through improvements in CT technologies and processes with focus on dose reduction (Webb et al. 2014*b*). It is this dose reduction both for the patient and the operators which is the main focus of this thesis.

Furthermore, the availability of CT scanner units has increased rapidly in most OECD countries over the past two decades (De Looper et al. 2009). Australia has the most number of CT scanners per capita, which is then followed by United States as demonstrated in Figure 2.4 followed by Greece, Denmark and Korea, all of whom had significantly more CT scanners per capita than the OECD average. Mexico, Hungary and United Kingdom had the lowest number of CT scanners per population. One contributing factor to the high number of CT scanners per capita in Australia may be geographical dispersion.

The ideal number of CT scanner units per population is difficult to estimate. While the lack of scanners may lead to patient access problems such as geographic proximity or waiting times, if there are too many scanners, this may then result in an overuse of these costly diagnostic procedures, with little if any benefits for patients and potential excess radiation exposure. Therefore monitoring and identifying solar radiation and nuclear radiation risks to the population is essential and monitored by government (Protection et al. 2000).

In Estonia, most CT scanners are installed in privately-owned diagnostic centers, and only a small number are found in public hospitals. With a lack of guidelines in place and minimum regulations that do not apply to private sector Estonia has topped the list.

Some evidence suggests that in the United States there is an overuse of CT examinations (Smith-Bindman et al. 2008). Between 1997 and 2006, the number of scans in the United States increased rapidly, while the instances of diseases remained constant (Smith-Bindman et al. 2008). Furthermore, in countries like Australia, payment incentives from Medicare allow doctors to benefit from exam referrals which may also be a contributing factor to overuse. However no conclusive evidence has been linked to the medical benefits of increased CT examinations in the United States (Baker et al. 2008).

Some OECD countries have been applying clinical guidelines to achieve a more rational use of diagnostic technologies such as CT scanners (*OECD Health Data* 2016). Diagnostic

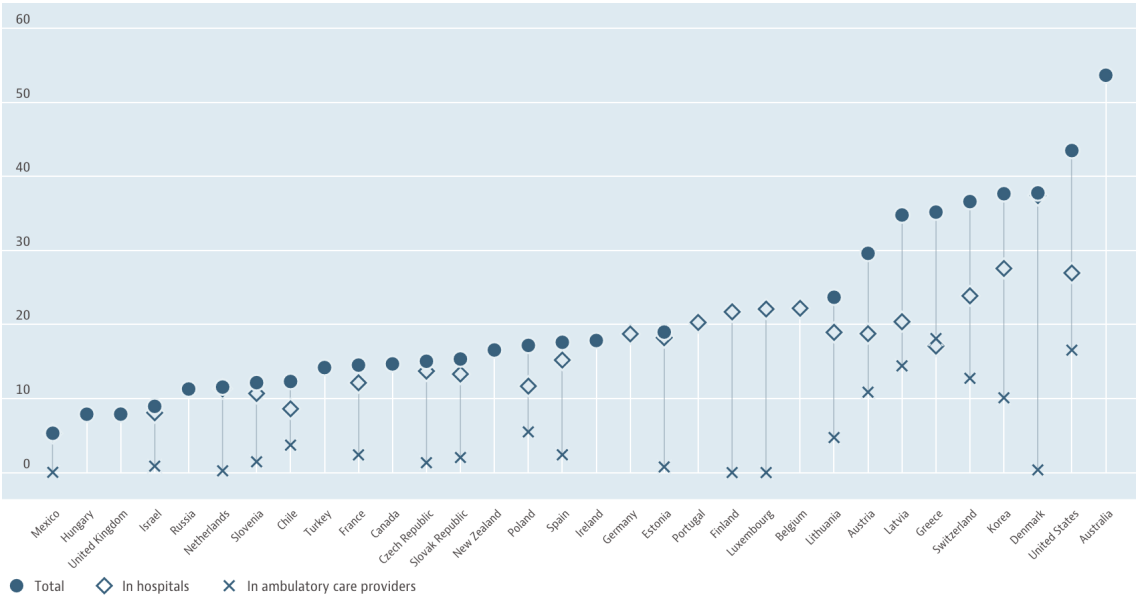

Figure 2.4: CT Scanners per million population OECD Health Data.

imaging is often used to guide a clinicians choice of the most appropriate examination. The objective is to increase the number of appropriate and safer examinations and reduce unnecessary high radiation and invasive examinations which may expose patients to risk without benefits (Bairstow et al. 2010).

2.2 CT Guided Biopsy Procedures

Biopsies are a useful and commonly used tool in medicine, whereby a tissue sample is taken in order to be externally analysed to test for diseases such as cancer. Biopsies on tissue near the surface of the body can be easily performed, however when the tissue is deep inside the body the biopsy becomes much more difficult. In these cases a CT guided biopsy may be undertaken. A CT scan provides a cross sectional view of the body, with a series of these images taken in what is known as a CT study, to visualise the location of both the suspect tissue and the needle being used to extract the biopsy sample.

One of the most useful applications of CT is guided surgical routines, where CT images assist in guiding the biopsy needle. CT guided procedures include biopsies where a sample of tissue needs to be extracted from patient's body using a biopsy needle for further analysis. Biopsy procedures can vary depending on the location of the lesion of interest. One

of the most common biopsy procedures are fine needle aspirations which are performed by passing a thin needle through the skin in order to sample fluid or tissue from a cyst or solid mass of the lung, liver, nodes or bones. There are also therapeutic injections of joints, nerve roots and epidural, radio-frequency ablation and drain placements (Seeram 2009). After the sample has been removed, it is transfered to a pathology laboratory where it is set in wax and finely sliced. The slices are then stained with various dyes that highlight different types and characteristics and abnormalities of cells.

Biopsy procedures involve inserting the biopsy needle at a predicted angle and advancing it along a desired path. This is a challenging task that requires practice and experience as well as sound judgment in spatial reference. To ensure the accuracy and safety of the procedure, radiologists typically advance the needle in a stepwise fashion, re-imaging the patient at each stage to determine any required corrections in trajectory (Shar et al. 2010). Steps currently involved in performing a freehand CT guided biopsy procedure include (Shar et al. 2010):

1. Positioning the patient, applying skin markers and performing a CT scan;
2. Assessing the image for safe biopsy path, measuring the desired entry angle and determining the skin entry point as depicted in Figure 2.5;
3. Marking the skin entry point on the patient;
4. Inserting the biopsy needle at predicted angle;
5. Advancing the needle in a stepwise fashion, re-imaging the patient at each step to determine any required corrections in trajectory Figure 2.6; and
6. Confirming the needle position prior to taking biopsy.

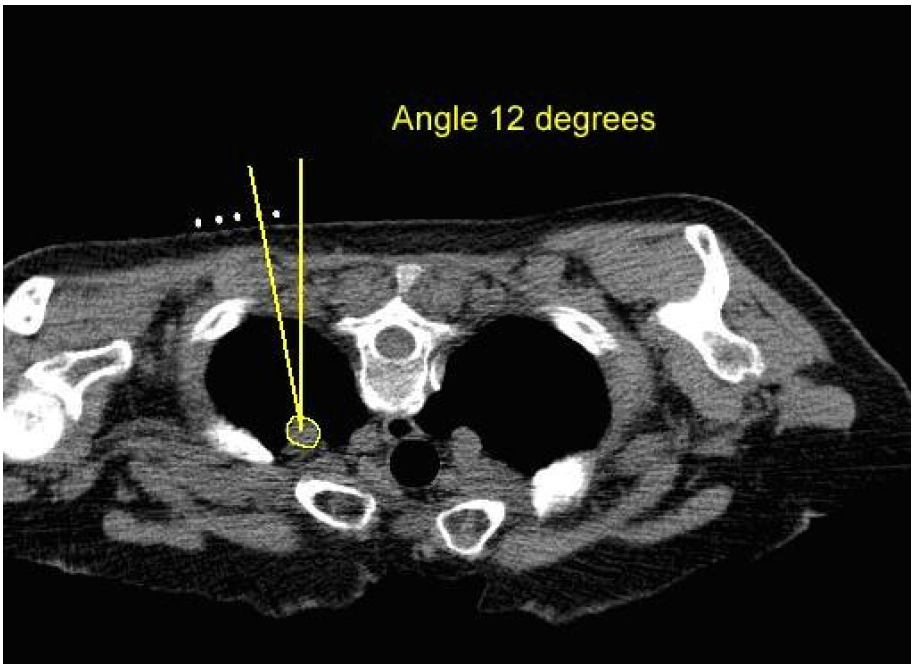

Figure 2.5: Biopsy path with the desired entry angle.

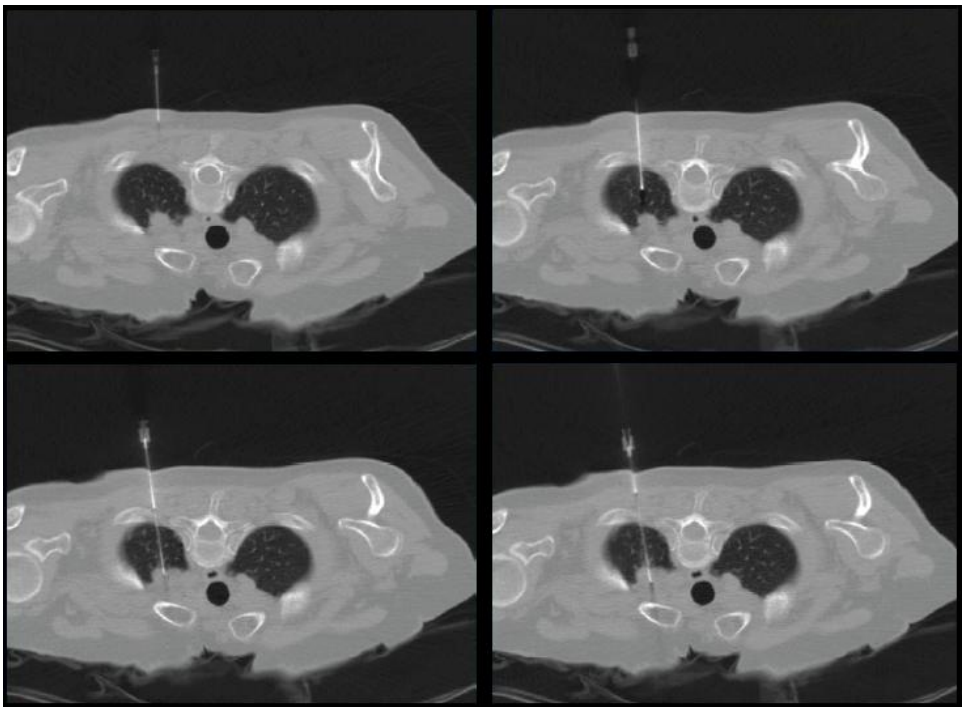

Figure 2.6: Advancing the needle in a stepwise fashion. This figure deminstrates the CT image in a standard medical format, DICOM. This figure demonstrates a cross sectional image of the body as well as the biopsy needle being inserted. It is clear why the CT images are crucial, as the specialist currently has no other way of visualising the needle location.

2.3 Biopsy Needle

A biopsy needle is used to obtain tissue or fluid samples which are then examined to determine malignancy. The biopsy needle usually includes a thin, long probe, called a stylet which sits inside a close-fitting hollow needle, called a cannula as depicted in Figure 2.7. Once the needle is inserted into the patient and is in position close enough to the lesion of interest, a firing device projects the stylet into the lesion of interest, and the cannula then follows immediately. The stylet comes with a notch where the tissue will prolapse once the stylet makes its way into the tissue. When the cannula then slides over the stylet, it severs the prolapsed tissue in the surrounding lesion of interest and then captures the prolapsed tissue like a specimen in the notch.

Figure 2.7: Core biopsy needle used to capture tissue from a lesion of interest.

For the purposes of this research, an infrared reflective tape was attached to the needle which then reflected the light back to the infrared camera capturing the location of the needle Figure 2.8. The reason why a reflective tape was used was because it was easily sterilised before each procedure and a very inexpensive and accurate method. The tape can be attached to all biopsy needles.

Infrared light is reflected back from the tape and then is picked up by the infrared camera demonstrating the location of the needle. The reason a tape has been utilised instead

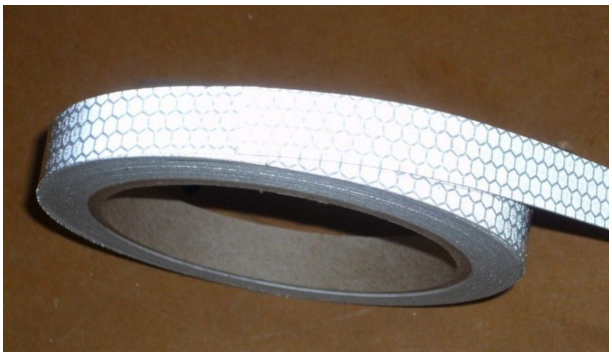

Figure 2.8: Infrared reflective tape which was attached to the needle and used to reflect infrared light back to the sensors.

of attaching a battery generated infrared light is mainly due to the fact that the tape can easily and more practically be sterilised. Another advantage is that the tape is non-metallic and so does not interfere with the CT operation.

2.4 CT Scanner Technology

A CT scanner shown in Figure 2.9 uses a motorised X-ray source that rotates around the circular bore of a CT scanner called a gantry. The CT technology is very different to conventional X-ray which uses a fixed X-ray tube. During a CT scan, the patient is positioned on a bed that slides into the gantry of the CT scanner while at the same time the X-ray tube rotates around the patient, exposing beams of X-rays through the patients body. Instead of film, CT scanners use Digital Radiography (DR) X-ray detectors, which are located directly opposite the X-ray source. As the X-rays go through the patient, they are sensed by the detector and then transfered to a computer where they can be viewed and manipulated (Hsieh 2009).

CT scanner technology has improved dramatically since the first scanner was introduced. Today's scanners can image the entire abdomen and pelvis of most adults, making a total of 300 CT images, in less than 10 seconds (Herman 2009). The amount of detail in the image has increased six-fold since 1970 as demonstrated in Table 2.1

CT technology has made great improvements since its introductions in the early 1970's. Advances in speed, patient comfort, and resolution have come a long way. The advances

Figure 2.9: Siemens Somatom Definition Flash.

Table 2.1: CT Scanner Technology.

CT Scanner Technology		
Specifications	First CT Scanner (circa 1970)	State-of-the-art CT Scanner (2016)
Time to acquire one CT image	5 minutes	0.5 seconds
Pixel size	$3mm \times 3mm$	$0.5mm \times 0.5mm$
Number of pixels in an image	6,400	256,000

in CT scanner technology mean that more anatomy can be scanned in less time. Faster scanning helps eliminate artifacts from patient motion such as breathing or peristalsis (muscle contractions). As a result of these advances, CT exams are now quicker and more patient-friendly than ever before. The advance in technology has lead to an increase in image quality, diagnostic confidence and a reduction in radiation dose. It is important to note that this thesis proposes a navigation system which would assist clinicians to perform a biopsy, it does not focus on speed or resolution of the CT technology.

A CT image is made up of an array of elements called pixels. Each pixel represents the mean attenuation of an axial column of the patients tissue about 1 cm in length as shown in Figure 2.10. A voxel is the square of the matrix times the thickness of the

image slice. Each time the X-ray source completes one full rotation around the patient, the CT computer then uses radiology specific software to construct a 2D image slice of the patient Figure 2.10. The thickness of anatomy demonstrated in each image slice can vary depending on the CT machine used, but usually ranges from 1-10 millimeters. During image acquisition the bed moves through the gantry while X-rays are produced, this results in helical data acquisition, which is then reconstructed by the software. This process continues until the desired anatomy is covered.

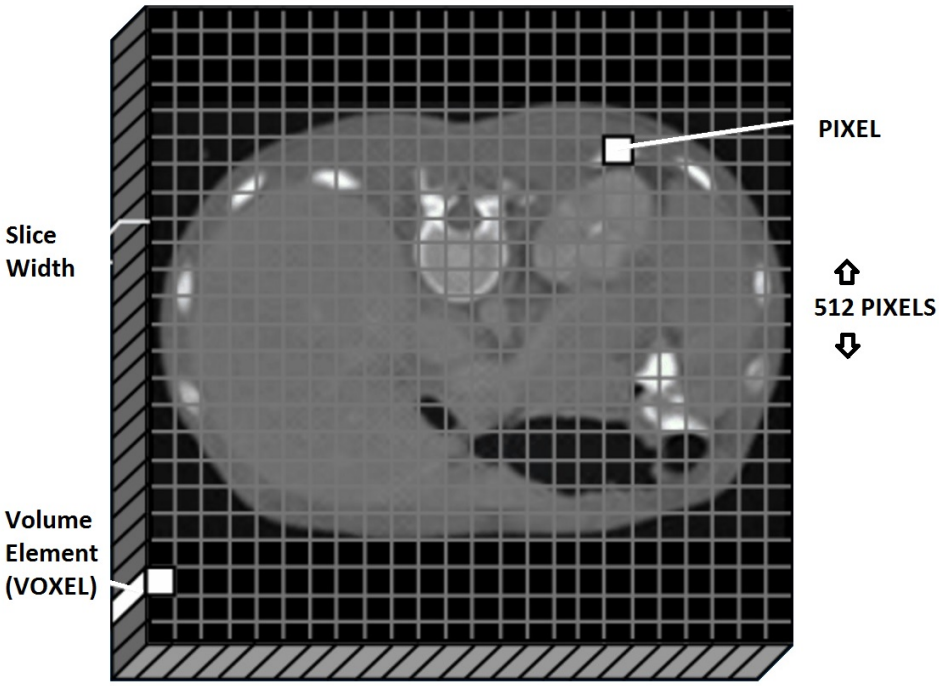

Figure 2.10: CT Slice consisting of pixels (*Physics Central* 2016).

Each time the X-ray tube and detectors rotate around the patient recording the radiation absorption by the patient's body, an image slice is generated as depicted in Figure 2.11. Software then computes and displays this information by assigning values to each pixel derived from the recorded data. Typically, a CT scan requires many X-ray photons (individual X-ray beams). Consequently, the amount of radiation used to make a CT scan is considerably greater than what is used to make a traditional X-ray.

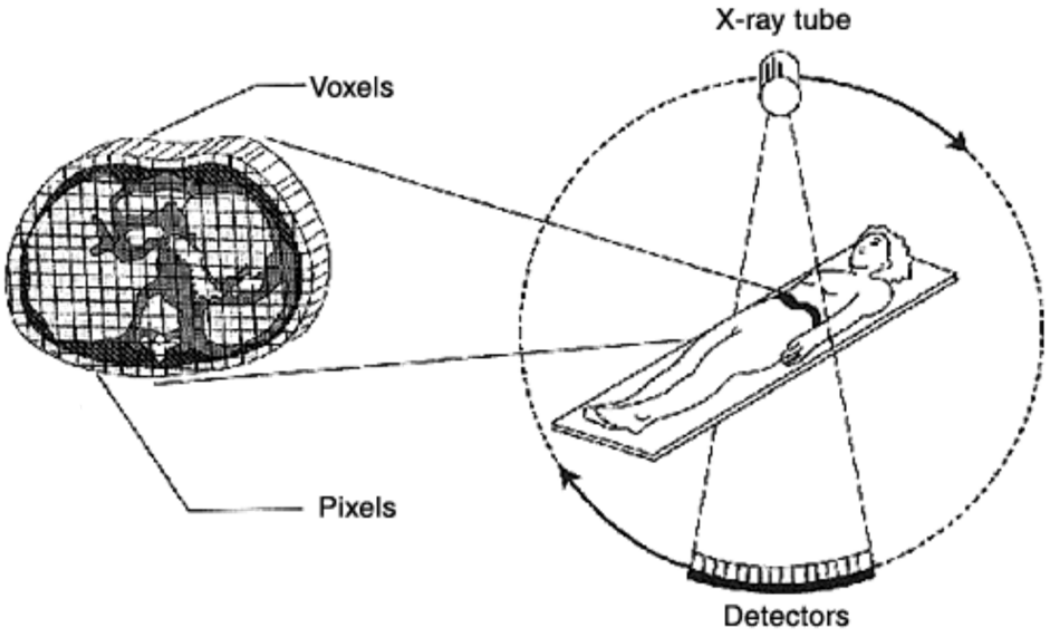

Figure 2.11: The X-ray tube and detectors rotate, with the axis of rotation running from the patient's head to toe (*Physics Central* 2016).

2.5 Digital Imaging and Communications in Medicine

DICOM stands for Digital Imaging and Communications in Medicine. It is an international standard related to the exchange, storage and communication of digital medical images and other related digital data (Graham et al. 2005). The main purpose of the DICOM standard is to allow cross-vendor interoperability among devices and information systems dealing with digital medical images, as long as all the involved devices comply with the DICOM standard.

Each DICOM file has a header section containing information such as patient demographics, acquisition parameters, referrer, practitioner and operator identifiers and image dimensions. The remaining section of the DICOM file contains the image data. A DICOM image file and it's header is depicted in Figure 2.12. The use of DICOM format and standard has been a major step forward in clinical radiology by allowing digital images to be easily stored and transferred electronically and also setting an industry standard which all medical imaging companies must adhere to. Digital images can be manipulated and converted to different formats for teaching and publication purposes.

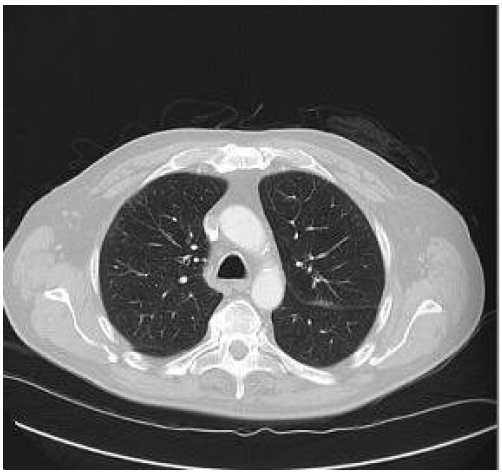

```
Grp  Elmt Length   | Description
-----------------------------------------------
0008 0005       10 | specific_character_set
0008 0008       28 | image_type
0008 0012        8 | instance_creation_date
0008 0013        6 | instance_creation_time
0008 0016       26 | sop_class_uid
0008 0018       42 | sop_instance_uid
0008 0020        8 | study_date
0008 0022        8 | acquisition_date
0008 0023        8 | image_date
0008 002a       20 | acquisition_datetime
0008 0030       14 | study_time
0008 0032        6 | acquisition_time
0008 0033       14 | image_time
0008 0050       10 | accession_number
```

Figure 2.12: A DICOM image and associated header. A DICOM header contains the patient and study information. The image is from a de-identified study which was obtained after receiving ethical clearance (Appendix F).

2.6 Radiation Dose

Background radiation exposure to humans is about 2.4 millisievert (mSv) every year which comes from the everyday radiation given off by the Earth as well as from outer space cosmic radiation or cosmic rays (UN 2008). In comparison, a CT scan has a radiation dose in the range of 1 mSv to 15 mSv and varies depending on the body part being scanned and specific techniques used. On average a CT of the chest is equivalent to having 100 chest X-rays (Pitman et al. 2009). This may appear to be a lot for one CT scan, however it still translates to a very small increased risk of developing cancer over a patient's lifetime. The risk is about a 0.04 per cent increase estimated by the Royal Australian and New Zealand College of Radiologists (Pitman et al. 2009). This means that if an individual has a 20 per cent lifetime chance of developing cancer, this rises to 20.04 per cent after a single CT scan.

The radiation dose for each X-ray modality and study depends on various factors including number of images (slices), patient build, number and type of scan sequences, and desired image resolution and quality (Žabić et al. 2013). The age of a patient and sex also are contributing factors. For example, breast tissue in women and the young cells in children are much more sensitive to radiation. Children have a higher risk of developing cancer because the results of radiation exposure might take a long time to appear. Unfortunately

most of the findings and calculations are largely based on data from survivors of atomic bomb explosions, rather than people who have undergone CT scans and X-rays.

In order to identify the amount of radiation dose delivered by CT scanning, various measures are, used including absorbed dose, effective dose, and CT dose index (CTDI) (Fischer, Battuello, Sadli, Ballico, Park, Saunders, Zundong, Johnson, van der Ham, Li et al. 2014). Energy absorbed per unit of mass is the absorbed dosage and is measured in grays (Gy). One gray equals 1 joule of radiation energy absorbed per kilogram. The level of risk to a particular organ is determined by the organ dose or distribution dose (Ogbole 2010).

The CT image quality would be much higher if the amount of radiation to patients was not taken into consideration. The higher the radiation the better the image quality but the more harmful for the patient. Thus the radiation received by a patient during CT scans are calculated to be a proportional estimate of the overall harm to the patient caused by the radiation exposure (Ogbole 2010). The effective dose, expressed in sieverts (Sv), enables comparison between different CT studies but it does not provide an accurate reflection of the true risk. For the purposes of estimation, the organ dose is the preferred method of measuring the absorbed radiation. Typically, CT doses are measured for a single slice (image) of the whole study and although useful for quality control, is not directly related to the organ dose or risk.

Organ doses from CT examinations are considerably higher than the conventional radiography examinations as identified in Table 2.2. For example, a typical anterior or posterior abdominal X-ray examination has a dosage of approximately 0.25 mGy, which around 50 times less than the corresponding stomach dose from an abdominal CT scan.

There are various contributing factors that determine the radiation dose for a particular organ during a CT procedure. The most important factor is the number of scans or examinations that a patient undergoes, the CT scanner's tube current and the time it takes to scan in milliamp-seconds (mAs), patient size, the axial scan range (for example an abdominal CT compared to a whole body CT), the scan pitch (the degree of overlap between adjacent CT slices), the tube voltage in the kilovolt peaks (kVp), and the specific design of the scanner being used (McNitt-Gray et al. 2002). Many of these factors are tailored to the type of study being performed and to the size of each patient and are

Table 2.2: Radiation Dose identifying different study types and associated organs with their relevant organ dosage.

Radiation Dose		
Study Type	Relevant Organ	Relevant Organ Dose (mGy)
Dental OPG	Brain	0.005
Chest radiography	Lung	0.01
Mammography	Breast	3
Abdominal CT	Stomach	10
Neonatal abdominal CT	Stomach	20

under the control of the radiologist or radiology technician. The quality of CT images will decrease as the radiation dose decreases, this means that there will always be a trade-off between high quality imaging and low doses of radiation (Mettler et al. 2000).

According to (Amis 2007), in the United States CT examinations contribute to almost one half of the total radiation exposure per capita. The total radiation dose received by the entire US population from CT has been used to estimate the chances of cancer incidence or mortality in the whole population (Brenner et al. 2007) (Einstein et al. 2007).

One study suggested that as much as 1.52 percent of cancers may eventually be caused by the radiation dose currently used in CT (Brenner et al. 2007). These estimates however are debatable since the cancer risk model used relies on the National Academies of Sciences report on the biological effects of ionizing radiation (Beir 2006), which suggests that because of the lack of of available data it is difficult to evaluate cancer risk in humans at low doses (less than100 mSv), which is about ten to 100 times higher than the effective dose from a typical CT examination (Yu et al. 2009). Another factor that was not taken into account is the actual benefit of the CT scan to the patient, specially when the majority of the total radiation dose from CT to the population was obtained by older or symptomatic populations. In this demographic, the health benefit of a CT scan far exceeds the estimated potential risk (McCollough et al. 2009). These risks are used to estimate variation across study types, patients, and institutions and estimate the Lifetime

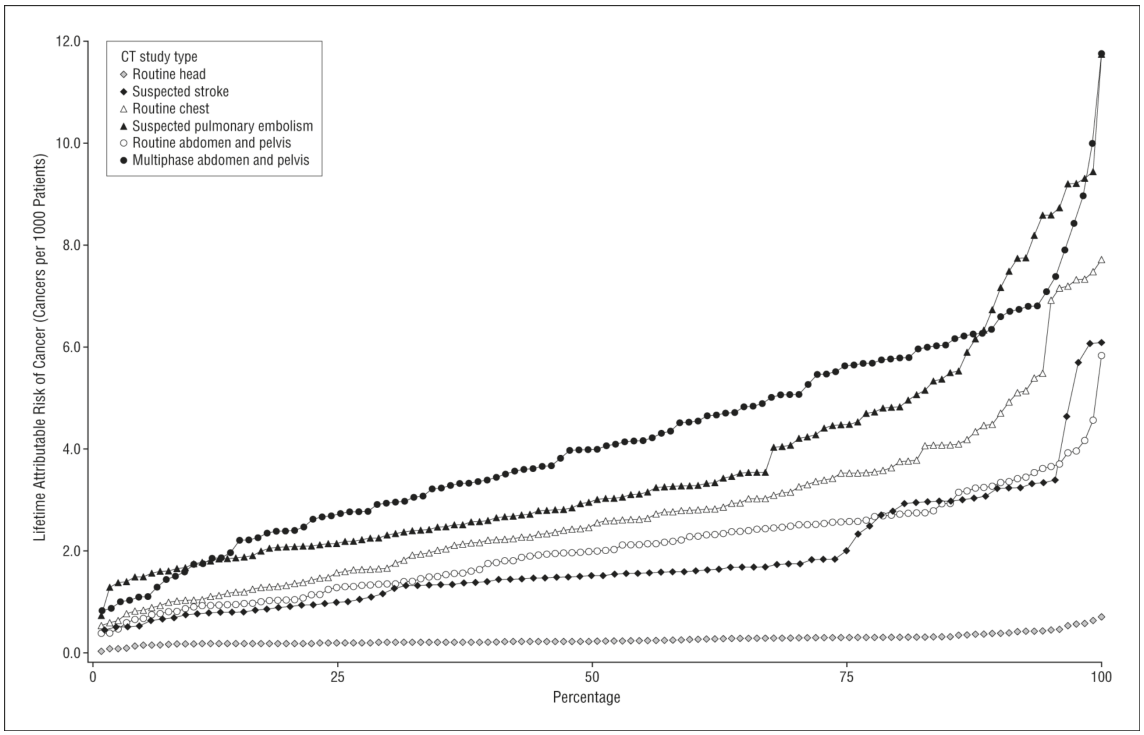

Figure 2.13: Estimated range in the Lifetime Attributable Risk (LAR) of cancer in a scenario where a 20 year old female patient has one of several types of computed tomographic (CT) exams. The x-axis represents the estimated effective doses for each study type, sorted from the lowest (1 percent) to the highest (100 percent) across patients (Smith-Bindman et al. 2009).

Attributable Risk (LAR) of cancer associated with these tests.

The estimated effective doses for each of the 6 most common CT study types, sorted from the lowest (1 percent) to the highest (100 percent) across patients, and the corresponding adjusted LAR of cancer are demonstrated in Figure 2.13, assuming all examinations were done on a 20 yeas old female patient. For a head CT scan, the average effective dose was 2 mSv, and the corresponding adjusted LAR of cancer was 0.23 cancers per 1000 patients (range, 0.03-0.70 cancers per 1000 patients). For a CT scan of multiphase abdomen and pelvis , the average effective dose was 31 mSv, and the corresponding adjusted LAR of cancer was 4 cancers per 1000 patients (range, 0.8-11.1 cancers per 1000 patients) as depicted in Figure 2.13 (Smith-Bindman et al. 2009).

2.7 Patient Trauma During Biopsy Procedure

Unlike surgery, the risks of CT guided biopsy are much lower. However, certain complications can still occur and include the following:

- Allergic reaction to contrast or dye are rare but do occur from time to time when iodine-based and also barium-sulfate contrast materials are used. These chemicals are essential to block or limit the ability of X-rays to pass through and as a result changing their appearance on CT images.
- Renal failure from the use of the contrast dye. Contrast Induced Nephropathy is a rare disorder and occurs when kidney problems are caused by the use of certain contrast dyes. In most cases contrast dyes used in a CT biopsy procedure have no reported problems. About 2 percent of people receiving dyes can develop complications. However, the risk can increase for people with diabetes, a history of heart and blood diseases, and chronic kidney disease.
- Infection. Skin is a natural barrier against infection. Even with many precautions and protocols to prevent infection in place, any procedure that causes a break in the skin can lead to an infection. These infections occur on the part of the body where the biopsy took place.
- Bleeding at the site tissue. Unexpected excessive blood loss may occur during a biopsy procedure. These losses are unexpected because the patient is not recognised as having a coagulopathy (condition in which the blood's ability to clot is impaired) and excessive because they are greater than is usual during such procedures.
- Pain during and post procedure. Local anesthetic is used during the procedure which prevents most of the pain. However often after the procedure patients experience some pain during the healing process.

2.8 Chapter Summary

This chapter introduced Computed Tomography (CT) and CT guided procedures and the tools used to perform these complex procedures including CT scanner technology. The use of DICOM imaging and its information header are explained. Then radiation dose and its impact on organs and likelihood of it causing cancer are discussed and some of the main complications and patient trauma that can occur during a biopsy procedure are outlined. The information stated in this chapter identifies the complexities involved in conducting a CT guided biopsy procedure and sets the groundwork for understanding different approaches to biopsy navigation.

Chapter 3

Approaches to Biopsy Navigation

This chapter begins with a review of existing approaches and techniques used in CT-guided biopsy procedures, including Gantry tilt techniques, patient positioning, angled and double angled biopsies. Some of the existing literature on biopsy needle tracking and the use of infrared technology in medicine is also reviewed.

3.1 Existing Approaches

After reviewing the existing tracking systems, it is evident that these systems are based on a number of different working principles and technologies.

3.1.1 Tracking Systems

The three main types of tracking methods currently used in surgical procedures are mechanical, electromagnetic and optical (Enquobahrie et al. 2008). Examples of these are shown in Figure 3.1and are summarized below (Shar et al. 2010).

1. Mechanical trackers are highly accurate and stable, but they are large in size and their use is limited to specific procedures where they will not interfere with the surgical routine (Kim et al. 2014).

Figure 3.1: Tracking system examples: mechanical, optical and electromagnetic trackers (Enquobahrie et al. 2008)

2. Optical trackers are, in general, not only more accurate than both the mechanical and electromagnetic trackers, but also tend to have a larger field of measurement. One of the major disadvantages of optical systems is that the line-of-sight between the trackers and the camera must be uninterrupted (Cleary et al. 2002).

3. Electromagnetic trackers use an electromagnetic field generator along with a number of small electromagnetic coils embedded in surgical instruments (Yaniv et al. 2009) which do not have the line of sight limitation (Fuangrod et al. 2016). The shortfall of electromagnetic trackers is that the surgical environment must be devoid of any ferromagnetic material that could interfere with the electromagnetic field and degrade the measurement accuracy. Another problem with electromagnetic trackers is that some of the surgical instruments need to be modified to include sensor coils.

After reviewing the existing tracking systems it is evident that optical tracking is a highly effective and accurate technique for localization with the only disadvantage being the maintenance of line-of-sight with the cameras and also the sterilization of markers. The infrared navigation system presented in this thesis uses more than one camera to address the line-of-sight issue and also uses infrared technology and reflector tape. The research presented in this thesis can potentially improve or even replace some of the current techniques outlined above.

3.1.2 Stereotactic Biopsy

Stereotactic biopsy is a biopsy procedure which uses computer technology and X-ray imaging to localise a target lesion such as a tumor or microcalcifications (calcium deposits) in the patients body in three dimensional space. Stereotactic core biopsy uses the parallax principle of measuring the angle of inclination between two lines to determine the depth or Z-dimension of the lesion of interest (Adam et al. 2014). In theory, any part of the body can be subjected to stereotactic surgery. However, difficulties in setting up a reliable frame of reference and also the time it takes to setup a stereotactic biopsy frame are some of the fundamental limitations. Stereotactic core biopsy is extensively used by radiologists specialising in breast imaging to obtain tissue samples containing microcalcifications. Figure 3.2 depicts a brain stereotactic setup.

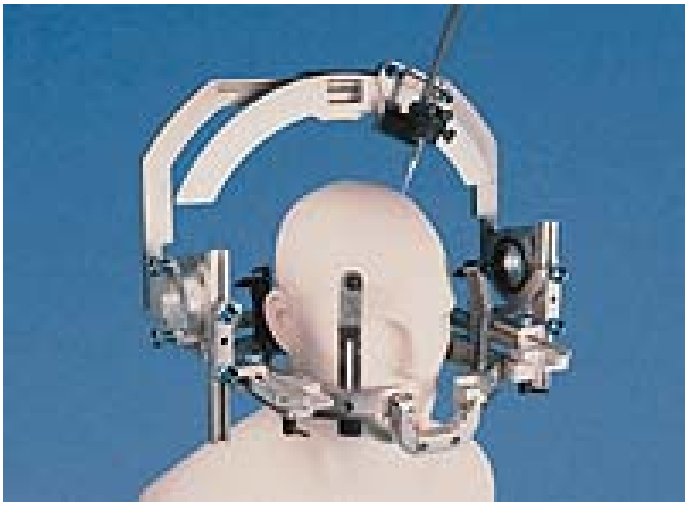

Figure 3.2: Steriotactic biopsy frame setup for a brain procedure (Markwardt et al. 2016).

For brain procedures, the main advantage of stereotactic CT procedure over other biopsy techniques is the stability and high accuracy which is required for biopsy of deep-seated lesions. X-ray-guided stereotactic biopsy is used for impalpable lesions that are not visible on ultrasound. A few days before the procedure a CT scan is taken and images are imported into a CT rendering machine which provides a 3-dimensional image of the brain and the lesion of interest. The 3-dimensional image along with a biopsy guidance arm is then used to guide the needle into the target.

3.1.3 Gantry Tilt Technique

During a biopsy procedure, the operator inserts the needle into the patient and advances it towards the lesion of interest, avoiding vital organs. A technique called gantry tilt technique is sometimes used to assist the operator.

Gantry tilt technique is used to tilt the CT gantry off the axial plane allowing the capture of CT images which demonstrate the appropriate path while avoiding vital organs and structures as depicted in Figure 3.3. The gantry tilt technique provides a degree of direct visualisation of the needle path towards the lesion on interest. The visualisation of the needle path is not possible with previously described methods such as stereotactic biopsy or the triangulation technique. The gantry tilt technique is a simple, practical way to perform angled CT biopsy or aspiration (entry of a foreign liquid, into the respiratory tract) cases.

Figure 3.3: Gantry Tilt of a CT Scanner (*Toshiba Healthcare - CT Technology* 2016)

.

3.1.4 Patient positioning CT-guided biopsy

During a biopsy, the operating radiologists can instruct the patient to take a certain position depending on the location of the lesion of interest. The prone position is often preferred as it limits chest wall motion (patient breathing) with an added benefit of a comfortable 'biopsy side down' post biopsy positioning of the patient (Cham, Lane, Henschke & Yankelevitz 2008). The supine position is associated with moderate chest movements, while the lateral decubitus position is associated with the highest chest movements. However, patient positioning is based on lesion accessibility and the safest path to the lesion

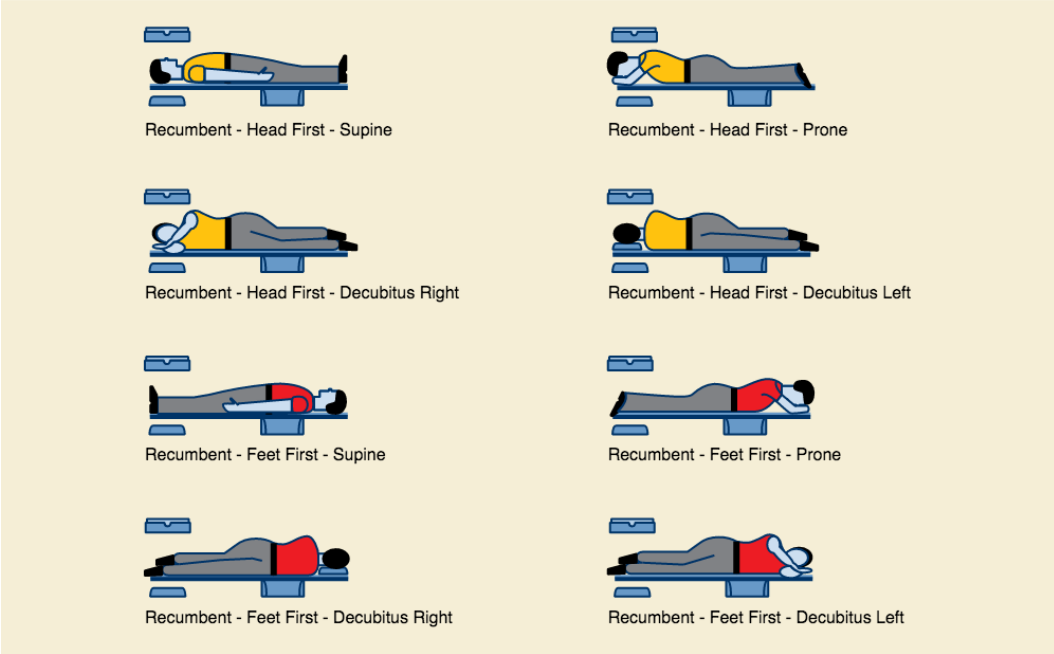

Figure 3.4: Illustrates different patient positioning techniques during a biopsy procedure (*Patient Positioning National Electrical Manufacturers Association* 2016).

of interest (Lal et al. 2012).

Patient positioning is important in improving the precision and safety of the biopsy as illustrated in Figure 3.4. If a lesion of interest is accessible from either prone, supine, or decubitus positioning, the prone position is usually the most ideal and offers more advantages. Human ribs, vertebrae and ligaments are configured in such a way that using the prone position would provide the least amount of chest wall motion when compared to supine and decubitus positions (Cham et al. 2008). The prone position also has the added advantage of allowing a more comfortable biopsy side down supine position during recovery, which may reduce the chance of developing a pneumothorax. The prone position also prevents the patient from seeing the biopsy procedure, which reduces both patient anxiety and patient movement (Cham et al. 2008).

3.1.5 Dual-angled CT-guided biopsy

Another CT-guided biopsy technique is the dual-angled CT-guided biopsy which employs angling both the CT-gantry and the patient to access the lesion of interest considered

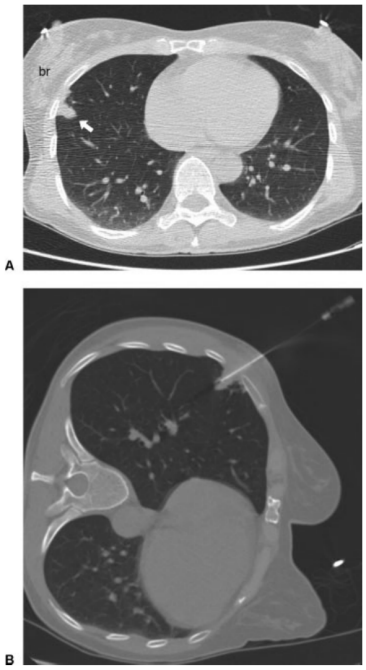

Figure 3.5: A. A lesion of interest in this case a right middle lobe peripheral nodule (arrow) is located deep to the right breast. B. The right breast is shifted medially by placing the patient in a left lateral position, allowing access to the lesion of interest (nodule) without traversing the right breast (Cham et al. 2008).

unapproachable using conventional CT techniques depicted in Figure 3.5. Angling the gantry and the patient, or dual angulation, can be applied for patients with masses located in areas not easily accessible. A dual-angled approach defines a safe path to a mass and allows obtaining a CT image in the plane of the biopsy needle (Sainani et al. 2013).

3.2 Literature Review

Radiological biopsy procedures have significantly expanded in the last twenty years thanks to the advances in CT technology and computing science. There are many potential applications of biopsy procedures and research is ongoing towards faster and more accurate approaches. As biopsy navigation is the focus of this thesis, this section begins with a review of previously proposed systems for CT-guided biopsy procedures, including tracking, robotic and visualisation solutions. The section goes then more deeply into the broad existing literature on infrared navigation and the tools and methods used in this research.

3.2.1 CT Guided Biopsy Systems

The diagnostic accuracy and clinical usefulness of CT-guided biopsies have been widely accepted as an effective and safe procedure to confirm the diagnosis in many clinical settings (Ozdemir et al. 2015, Frederiksen et al. 2015, Guimaraes et al. 2003, Galluzzo et al. 2015). The advantage of CT guidance is that the whole abdomen is visualised, and this allows accurate planning of a biopsy for deep-seated lesions. In recent years, the efficacy of CT-guided biopsy for making the pathological diagnosis of lymphoma has been reported as both the biopsy techniques and the histological diagnostic techniques have dramatically improved (Sklair-Levy et al. 2000, Demharter et al. 2001, Pappa et al. 1996).

The problem of camera calibration for metric extraction has been addressed over many years by several authors, with extensive literature on the subject (Hartley et al. 2005). The area has historically attracted interest from two separate perspectives: computer vision (Medioni & Kang 2004) and photogrammetry (Babapour et al. 2016).

A robotic system where the whole procedure was intended to be performed with the patient inside the scanner was proposed by (Elhawary et al. 2010). The biopsy probe incorporated a surface coil and two semiactive markers. The system used two scan planes, sagittal plane and plane through the marker, for automated tracking of the probe. Unfortunately, clinical results showed that the targets located in the peripheral zone of the prostate were not accessible because of the limitations in the angular movements of the probe due to the mechanical design of the robot and probe design.

A study was performed (Groetz et al. 2015) to evaluate the feasibility of CT-guided biopsies using a novel robotic needle guide. Eight vertebral bodies of dead swine were biopsied, the operators attempted to place the needle in the center of the vertebral body via a transpedicular access. Needle placement was accurate without any need for readjustment. it was concluded that the system may offer even less experienced teams to take biopsies in regions which are difficult to access.

An electromagnetic navigation system for CT guided biopsy of small lesions was proposed by (Gruber-Rouh et al. 2015*b*). These devices increase accuracy and lower radiation exposure during CT-guided puncture without restricting patient accessibility. Similarly

(Leong et al. 2012) proposed an Electromagnetic navigation system for CT-guided biopsy of small lesions used a phantom study which demonstrated that fewer passes and decreased amount of time is required to reach small targets in the lung when using electromagnetic tracking vs conventional CT.

A percutaneous lung biopsy where comparison between an augmented reality CT navigation system and standard CT-guided technique where conducted by (Grasso et al. 2013). The device can be used for percutaneous interventions such as biopsy, thermal ablation, percutaneous interventional, localisation and positioning of fiducials for radiotherapy in different anatomical districts, such as lungs, bones and kidneys. It reconstructs a 3D model from a data set of acquired CT images through automatic procedures.

A phantom study to examine a real time electromagnetically guided navigation system and performed comparisons to standard computed tomography (CT) guidance was conducted by (Moncharmont et al. 2015). A prospective, randomised, comparative study was conducted. Clinicians without prior experience on the new navigation system attempted to biopsy two 6 mm-diameter targets with out-of-plane trajectories using both the standard CT-guided method and the new navigation method. The clinicians consistently performed faster and more accurate phantom biopsies with out-of-plane trajectories using the electromagnetically-guided navigation system than with the standard CT-guided method. This research suggests that CT guided biopsy procedures alone are not the most effective approach.

In order to evaluate the accuracy and clinical relevance of a free-hand, CT-guided, optical navigation system, 15 procedures in 14 patients were analysed (Schubert et al. 2013). The navigation system was applied for interventional procedures on small lesions of interest, and none of the evaluated parameters correlated significantly with the distance from the needle tip to the planned target. The application of a navigation system for CT-guided procedures proved safe and provided an effective targeting within a reasonable intervention time (Gruber-Rouh et al. 2015*b*)

Numerous navigation systems used for ablation (removal of body tissue) are reviewed, and specific clinical applications for ablation are discussed to help define how these technologies address specific clinical needs, and fit into clinical practice (Wood et al. 2010).

An electromagnetic navigation system is evaluated for CT-guided biopsy of small lesions (Appelbaum et al. 2011). Standardised CT anthropomorphic (human like) phantoms were biopsied by two radiologists. CT scans of the phantom and surface electromagnetic fiducial markers were imported into the memory of the 3D electromagnetic navigation system. Virtual electromagnetic tracking appears to have high accuracy in needle placement, potentially reducing time and radiation exposure compared with those of conventional CT techniques in the biopsy of small lesions.

3.2.2 Infrared Technology in Medicine

Infrared technology has long been used to monitor and measure the temperature distribution of human skin. An infrared thermogram is used to identify diseases such as malignancies, inflammation, and infection because of localised increases in temperature as hot spots or as asymmetrical patterns. When thermographs are used under controlled conditions, they may be interpreted readily to diagnose certain conditions and to monitor the reaction of a patient's physiology to thermal and other stresses (Jones 1998).

The Nintendo Wii Remote infrared sensor illustrated in Figure 3.6 was chosen for this research due to availability, cost effectiveness, ease of interfacing, and high resolution. The infrared sensor on the Wii Remote is capable of tracking up to four IR hot-spots simultaneously, with positions output at 100Hz in 1024 by 768 interpolated resolution (Lee 2008). Only the positions and size/intensity of the IR hot-spots is output, with the raw video output from the sensor not available. A Bluetooth interface is included on the Wii Remote to enable communication.

Figure 3.6: Nintendo Wii remote infrared camera used in this research (Lee 2008).

Infrared technology has proven useful in various applications in medicine, some of which include:

- Identifying blood vessels in laparoscopic surgery: During surgeries where a fibre-optic instrument is inserted through the abdominal wall to view the organs in the abdomen or permit small-scale surgery surgery it can be hard to identify blood vessels. Near-infrared spectroscopy sensors can be installed into the tips of surgical cutting tools enabling surgeons avoid cutting blood vessels accidentally (Eggers et al. 2015). The sensors on the device detect the presence and diameter of blood vessels in laparoscopic surgery alerting the surgeon to their presence and locations.
- Blasting cancer cells: Destroying cancer cells without harming healthy cells is a big challenge when it comes to cancer treatment. A method where Nanoparticles are injected into the bloodstream with a purpose of finding lung cancer cells has been developed (Nie et al. 2007). Cancer cells absorb the nanoparticles and an infrared light is then projected onto the relevant area, where the nanoparticles absorb it and convert the light into heat and destroy the cancer cells.
- Detecting bed sores: Near-infrared light used to reduce infections in the hospital environment. A system that identifies bed sores before they actually appear on the

skin (Lloyd et al. 2010). The infrared light is emitted onto to the skin. The device measures hemoglobin concentration and oxygenation beneath the surface of the skin to help physicians assess tissue damage indicating early signs of bed sores.

- Sepsis (harmful bacteria) detection: A breath biomarker developed by Isomark (Schober et al. 2011) is part of the key to its early detection. When the body has an infection, it tends to use a specific carbon (carbon 13). Patients exhale into a bag where spectrometer equipped with infrared lasers measure the ratio between carbon 12 and carbon 13. Early detection and treatment of sepsis is then made possible.

3.3 Chapter Summary

In this chapter some of the existing approaches used in CT guided biopsies was described. Then a review of literature was presented where existing CT biopsy and infrared technologies were reviewed. Some of the attributes that set this system apart from other technologies and techniques available in health care include the use of multiple cameras to track the biopsy needle during the procedure and the utilisation of infrared technology and reflective tape which can be sterilized much easier and quicker than other means. This research focuses on addressing the lack of spatial referencing during the procedure and also included the design and testing of a training module where clinicians can practice biopsy procedures using the system.

IR reflectors were considered for this application, however because of the below reasons were deemed not appropriate at this time:

1. The IR camera does not pick up more than 4 hot-spots at a time.
2. The software works best when the strongest IR hot-spots is picked up from each camera. The needle recognition rate is better when only the strongest point is picked up.
3. After consultation with clinicians, reflective tape was identified as more easily sterilisable.

4. Super gluing multiple metal hot-spots onto a patient would be very time consuming and at times not practical.

The next chapter focuses on presenting the navigation system used in this research. Robustness of some of the methods are investigated and shortfalls identified. In Chapter 4, a proof of concept identifies the the need for an infrared navigation system, and a review of clinical trials is presented.

Chapter 4

Design of the Multiple-Camera Infrared Navigation System

This chapter describes the hardware and software used to run and operate the infrared guided biopsy navigation module. Including infrared cameras and their calibration method, system mapping and interface establishment between the infrared cameras and emitter. This chapter also covers multiple camera mapping.

4.1 System Components

The infrared guided biopsy needle system provides a method to estimate needle trajectory and position using computed tomography image points and multiple infrared measurements. The system includes a digital infrared-sensitive camera and high-intensity infrared illuminator, which is used to capture the position of an infrared reflective tape attached to a coaxial biopsy needle having been inserted into a marked insertion point on a test phantom. Information is then sent in real-time to a custom software program where needle entry position is displayed and coordinates captured as shown diagrammatically in Figure 4.1 and demonstrated in Figure 4.2.

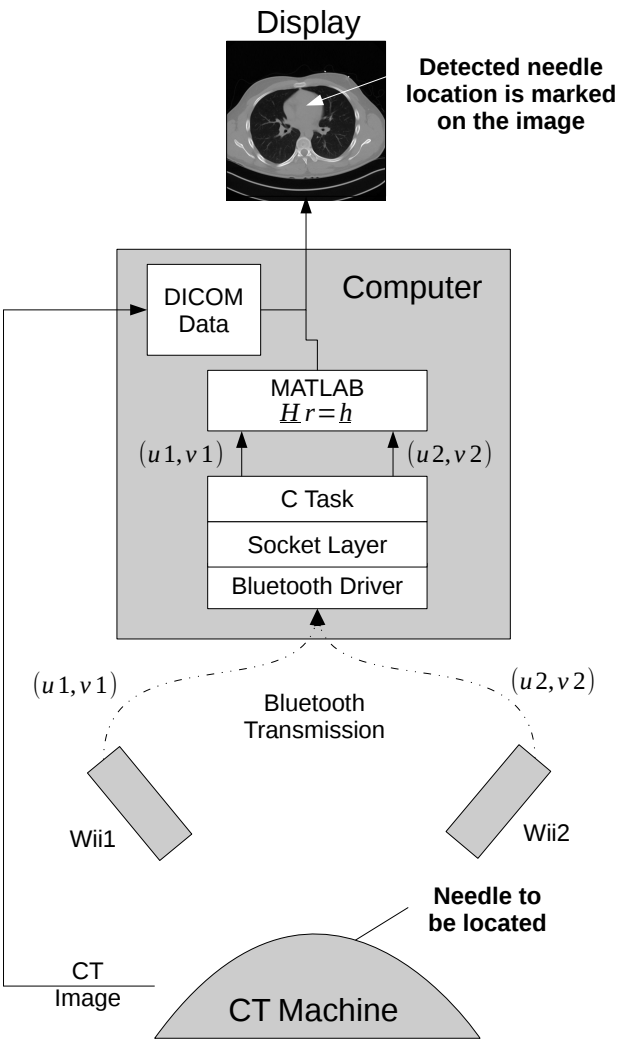

Figure 4.1: A block diagram demonstrating the setup and interfaces. Two infrared cameras connected via bluetooth to software which display the location of the biopsy needle.

The communication thread in the interface application first opens and binds to a Unix inter-process communication (IPC) socket which acts as a data communications endpoint for exchanging data between processes executing on the same host operating system, waits for the client application to connect, then enters a command/response loop. Command packets sent from client to interface application consist of a single byte, with 'd' indicating a request for data and an 'x' indicating exit.

An interface application was written (Listing 4.1) to communicate with and configure the Wii Remote and access the IR hotspot position data, and a client program in MATLAB

Figure 4.2: Top: System setup including infrared emitters, wii cameras fixed and a phantom with entry marks. Bottom: The biopsy needle with infrared reflective tape attached.

to provide additional abstract functionality. The interface program spawns three threads – two responsible for interfacing with the Wii Remotes, and the last for communicating with the client program. Interfacing with each Wii Remote is performed using generic Bluetooth libraries, and input and output sockets. The 'wiiuse - The Wii Remote C Library' was used as the drivers for the system (Appendix E). These drivers are registered to the device driver access point, where the device is read from using MATLAB code (Listing 4.1) by loading the Wii Remote drivers to kernel, connecting from client application to drivers, request data from the Wii Remote, processing and decoding and plotting the incoming data.

Listing 4.1: Steps that the custom software takes when activated.

```
1. Load Wii Remote drivers to kernel
2. Connect from client application to drivers
3. Request data from Wii Remote
4. Process and plot data from Wii Remote
5. Repeat steps 3 and 4 until the client program is closed
```

4.2 System Interfacing

An interface application was designed and tested to communicate with and configure the Wii Remote Infrared (IR) cameras and access the IR hotspot position data as demonstrated in (Listing 4.2). There is also a client program in MATLAB to provide additional abstract functionality. Interfacing with each IR camera was performed using generic Bluetooth libraries (Lee 2008), and input and output sockets.

The followings steps are performed on launching the interface application:

1. A prompt is displayed for the user to make the Wii Remotes discoverable;
2. A socket connection is established with the Bluetooth HID (human interface device) on the host computer;
3. A scan for Bluetooth devices is performed, and input and output sockets created to connect to any discovered Wii Remotes;
4. The socket connection to the Bluetooth HID is closed;
5. Two polling threads are created and capture of IR data from the Wii Remotes started;
6. The user is prompted to assign left and right positions via button presses on each Wii Remote;
7. A client communications thread is created, and the user prompted to start the client program.

Listing 4.2: Custom MATLAB Program - reads and plots coordinates x and y. Some lines are removed for clarity.

```
fid = fopen('/dev/Wii Remote','r');
n=0;
tline = fgetl(fid);    //returns the next line of the specified file
while ischar(tline)
    disp(tline)
    tline = fgetl(fid);  // reads characters
end

function [ wii ] = demo()

        coord.ir.x(:,1:end-1) = coord.ir.x(:,2:end);
        coord.ir.y(:,1:end-1) = coord.ir.y(:,2:end);
        plot(coord.ir.x(1,:), coord.ir.y(1,:),'rx');
        plot(coord.ir.x(2,:), coord.ir.y(2,:),'bo');
end
fclose(fid);
```

The response packet is 24-bytes for each Wii Remote, for a total of 48-bytes. Each 24-bytes of data from each Wii Remote consists of 6-bytes for each IR hotspot – two-bytes each for the u and v-positions, and two-bytes for size/intensity.

The client application was written in MATLAB to facilitate post-processing of the sensor inputs into meaningful surgical guidance co-ordinates and this is the subject of Chapter 5. A socket connection to the interface application is established, and a display window opened containing a plot of the IR hotspots. A loop is established that sends request packets, receives response packets, and calculates (x, y, z) coordinates for each of the two most intense hotspots. The loop exits, and the interface and client programs close, when the display window is closed by the user. The (x, y, z) coordinates for each hotspot and the method for estimating the projection parameters is described in Section 4.3.

4.3 Calibration

An aluminum jig was machined to enable precise, repeatable location of two Wii Remotes in a binocular configuration Figure 4.3. The jig aligns each Wii Remote using the upper (the face containing the majority of the buttons), one side, and end face. The Bridgeport milling machine used to machine the jig was also employed to calibrate and estimate the projection (camera) parameters of Equation (5.65) as explained further in section 5.4.1.

Figure 4.3: An aluminum jig $165mm \times 95mm$ was machined to enable precise, repeatable location of two Wii Remotes in a binocular configuration

First, the focal length of the Wii Remotes and exact position of the IR sensors within them are unknown. As such an arbitrary reference origin was chosen, and the projection parameters calibrated with respect to this.

In order to estimate the projection parameters, the client application was modified to accept user input of (x, y, z) coordinates then collect 100 data points from each Wii Remote. The Wii Remote jig was positioned square to the mill at a distance of approximately a metre, and a single IR LED mounted to the mill table. The milling machine is capable of positioning an object to a precision of 0.01mm, with accuracy better than 0.05mm (positioning accuracy is closer to the 0.01mm precision when not machining).

Forty-three positions spanning a range of ±100mm along each axis were collected, with 25 positions in the x-y plane corresponding to the designated zero z-coordinate, and 9 positions in each of the planes corresponding to the ±100mm z-coordinates. Outliers were removed from the collected (u, v) values, the mean of the remaining (u, v) values taken, and Equation (5.73) used to solve for the projection parameters. The mean was used rather than the median to allow average (u, v) values to fall between the integer constraints imposed by the pixel values.

The mill was used during these experiments to machine the items. There is a head or turret where the cutters are loaded, and a movable bed where the workpiece is attached. The bed can be manually adjusted in the x, y and z directions to a precision of 0.01mm. The WiiMote and IR source were attached to the turret and bed respectively and move one relative to the other. The x and y axes used optical sensors to provide a digital readout of 2D position to 0.01mm, while the z-axis has a dial readout that is around 0.02mm.

4.4 Chapter Summary

This chapter outlined the system setup. It identified the system components and the steps performed on launching the interface application. The interface application and how it communicates with and configures the infrared cameras were explained. The chapter then continued to describe the calibration method using an aluminum jig configuration to enable precise location. In next chapter the transformation of the multi-camera points onto the DICOM images are examined.

Chapter 5

Camera Mapping Algorithm Design & Image-Based Guidance

This chapter starts by evaluating the need for a biopsy guidance system, conducting simulated CT biopsies of targets within a phantom by attaining a vector by subtracting the current location of the detected spot from the starting location, and using that vector as the angle. A 2D to 3D transformation of the system and the development of a new infrared guided biopsy method where two infrared cameras are used to navigate are described, and the chapter then examines the 3D version of the system. After a review of clinical trials, a further developed 2 x 2D system is developed and investigated.

5.1 The Need for a Guidance System

In order to identify whether the proposed infrared guidance system would improve accuracy and be beneficial in a biopsy procedure, a biopsy simulation and training module (Appendix D) was constructed. The main purpose of this initial experiment was to provide a proof of concept. To identify if guided biopsy achieves more accurate results when compared to freehand biopsy results. The system comprised of a biopsy needle with an infrared reflective tape on its hub, an infrared illuminator and detector as well as a laptop computer as depicted in Figure 5.1. The infrared detector was connected via Bluetooth

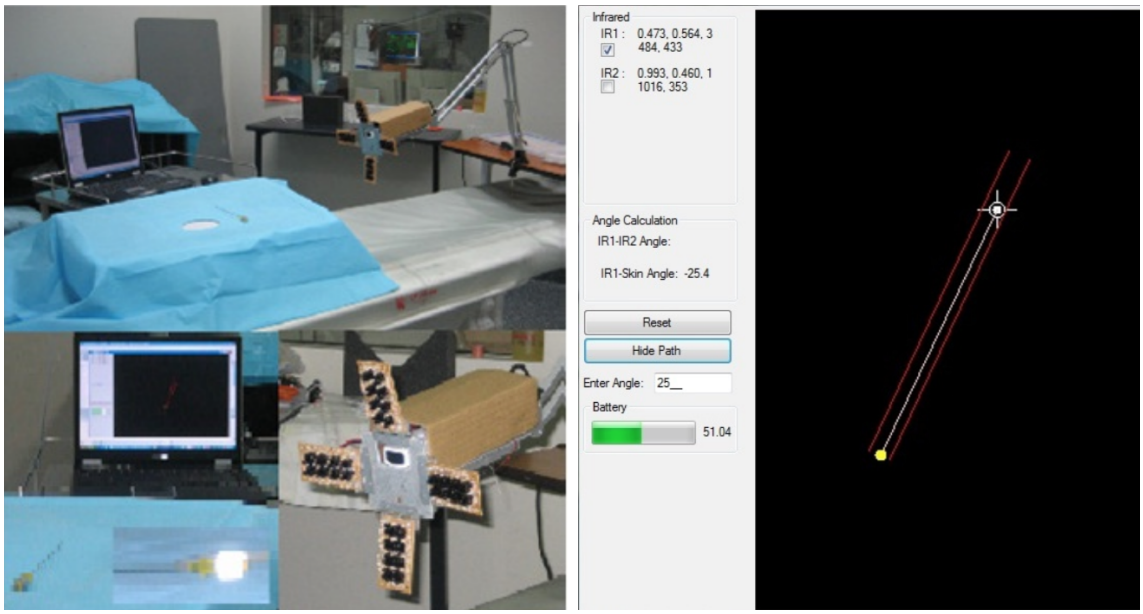

Figure 5.1: Initial system setup, which is comprised of a biopsy needle with an infrared reflective tape on its hub, an infrared illuminator and detector as well as a computer with custom software. The infrared tape on the needle hub is identified in the picture traveling down a path towards the lesion of interest identified as a yellow dot.

to the computer which had running a tracking software specifically designed, written and tested for this purpose. The needle position with respect to the biopsy target was updated in real-time and displayed on a computer screen as feedback for the trainee operator facilitating accurate angle positioning of the biopsy needle (Shar et al. 2010).

Simulated CT biopsies of targets within a phantom were conducted, alternating freehand and infrared guided techniques with the axial angular error statistically compared (Appendix A). The experiment was conducted over two sessions using both freehand and infrared guided approaches. In the infrared process, the operator first made the entry point on the phantom and captured the position using the infrared camera and computer software (Shar et al. 2010). They then entered a desired insertion angle and calibrated the path to the lesion using the software. The biopsy needle was then inserted into the phantom by the operator guided by the feedback from the monitor screen, thus enabling real-time trajectory corrections, with achieved angles recorded on a computer (Shar et al. 2010).

The setup was orchestrated in a way to mimic real biopsy procedures which regularly take place in that environment using the same CT scanner. The operators who assisted in the experiments were trained radiologists who perform biopsies on a regular basis.

During the experiments both the actual (the angle which the operator was going for) and outcome angles (the angle which the operator recorded) were recorded for later analysis, which was in the form of correlation analysis (Kreyszig 2010) the details of which are presented below. Let us consider n ordered pairs of samples, $\{(x_j, y_j)\}_{j=1}^{n}$, each consisting of an actual and outcome angles, x and y, respectively. Then, the sample means for the actual and outcome angles are computed as

$$\bar{x} = \frac{1}{n}\sum_{j=1}^{n} x_j \tag{5.1}$$

and

$$\bar{y} = \frac{1}{n}\sum_{j=1}^{n} y_j \tag{5.2}$$

respectively. The respective samples variances are then

$$s_x^2 = \frac{1}{n-1}\sum_{j=1}^{n} (x_j - \bar{x})^2 \tag{5.3}$$

and

$$s_y^2 = \frac{1}{n-1}\sum_{j=1}^{n} (y_j - \bar{y})^2 \tag{5.4}$$

while the sample covariance is given by

$$s_{xy} = \frac{1}{n-1}\sum_{j=1}^{n} (x_j - \bar{x})(y_j - \bar{y}) . \tag{5.5}$$

The sample correlation coefficient, r, which is a measure of the degree to which x and y are linearly related (Kreyszig 2010), is computed through

$$r = \frac{s_{xy}}{s_x s_y} \tag{5.6}$$

where $-1 \leqq r \leqq 1$, with $r \approx 1$ indicating strong positive correlation between x and y, a positive negative change in x results in positive (negative) change in y, while for $r \approx 0$ indicates that there is little or no linear relationship between x and y. The ideal result for a guidance system considered here would be strong positive correlation, which would imply highly accurate biopsy insertions.

The verification results of this preliminary evaluation are given in Figure 5.2 and outlined in (Appendix A) where the user attempts to keep the number reported by the system to a target. Actual angles are plotted against outcome angles recorded during the experiment. The outcome angles for the proposed infrared-guided approach were found to be closer to the actual angles, than those achieved by the freehand approach. This was was confirmed using correlation analysis.

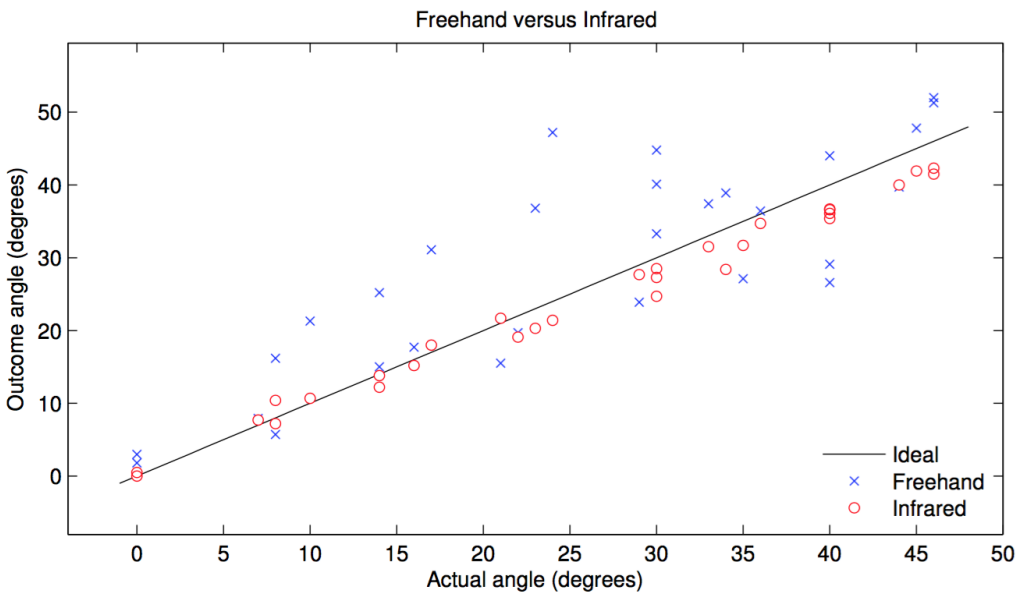

Figure 5.2: Results of simulated CT guided biopsies by freehand and infrared guided techniques.

The freehand approach achieved $r = 0.8382$, while the infrared method achieved $r = 0.9948$, where r denotes the correlation coefficient (Kreyszig 2010). For the purposes of analysis a number of statistical tests were used given in with level of significance p set to 0.05. Using absolute values in 30 trials, infrared was closer to true angle than freehand 25 times. A binomial test indicates that there is a vanishingly small probability of 25 successes in 30 trials under the null hypothesis of no difference in success rate between these two methods (Shar et al. 2010). Thus, the infrared guided technique achieved a significantly higher success rate than the freehand as demonstrated in Figure 5.2. Both the mean and median differences between each method and the true angle were smaller for infrared than freehand, also indicating that the infrared method is more accurate (Shar et al. 2010).

Using signed values the range of the differences was smaller for infrared than freehand, again showing that the infrared method is more precise as demonstrated in outlined in (Appendix A) where actual angles and outcome angles are compared. The sign test rejects the null hypothesis that the infrared and freehand median differences are equal. Given that infrareds median difference is smaller, infrared is confirmed as superior in this case. An explanation as to why data may not be distributed normally is extreme values in a data set. During the biopsy procedure, the camera may be blocked by hand movements and as such extreme values may be recorded. Assuming that the dataset is normally distributed, the paired t-test was employed, with the result that this also suggests that the infrared guidance method is superior to the freehand method (Shar et al. 2010). The paired t-test only requires an approximate normal distribution, which is not an unreasonable assumption given the closeness of fit shown in Figure 5.2. The presence of a significant number of outliers may invalidate the use of this test, but this does not appear to be the case given the experimental data available. Therefore, the conclusion that the infrared guidance system is somewhat superior to freehand guidance is supported.

5.2 3D System

Given the success of the angular IR measurement described in the previous section, the approach was extended into 3-dimensions in order to determine whether further improvements could be made in clinical guidance accuracy. The client application was further developed to two cameras and converted into MATLAB programming language which allowed for more accurate plotting of IR results and better user interfaces. A socket connection to the interface application is established, and a display window as depicted in Figure 5.3 is produced, containing a 3D plot of the IR hotspots. A loop is established that sends request packets, receives response packets, and calculates (x, y, z) coordinates for each of the two most intense hotspots. The loop exits, and the interface and client programs close, when the display window is closed by the user. The (x, y, z) coordinates for each hotspot are calculated using Equation (5.83) as will be developed in section 5.4.2.

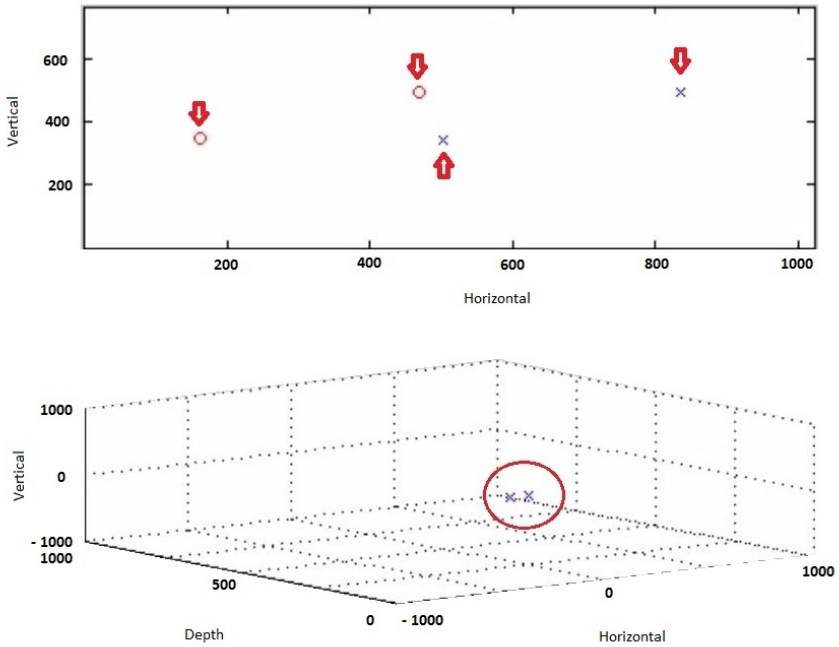

Figure 5.3: The 3D Visualisation Tool: The upper plot shows the raw (u, v) coordinates returned by the Wii Remotes (crosses are from the left sensor and circles from the right). The lower plot is the (x, y, z) mapping of the (u, v) data for the two IR sources.

5.2.1 Mapping Algorithm

Given the requirements for mapping and calibration, and the need to have a simple and semi-automatic calibration system, the application of Zhang's methods is investigated for this problem (Zhang 2000). The projection system according to Zhang's result is defined, and subsequently extended to the case of two IR cameras. The basic problem may be summarized for one camera by referring to Figure 5.4. The observed camera point $\mathbf{m}$ corresponds to 3D point $\mathbf{M}$, but the mapping is not unique. Using some preliminary tests that were conducted using the training module and CT scanner, the raw (u, v) coordinates returned by each of the the Wii Remotes and the corresponding (x, y) mapping of the (u, v) data for the two IR sources demonstrated a correlation (Appendix B).

Consider, for example the situation where the camera (that is, the projection plane) is moved further away. The mapped point in the image plane may not alter. Thus, it is clear that at least two cameras are required to fully resolve the ambiguities. One approach is to utilize the precise knowledge of the camera position, comprising its center (u_0, v_0)

and orientation with respect to the real-world XYZ axes. Furthermore, the scaling with respect to the real world is required. In general, this information is not available; in our situation, it is impossible to acquire.

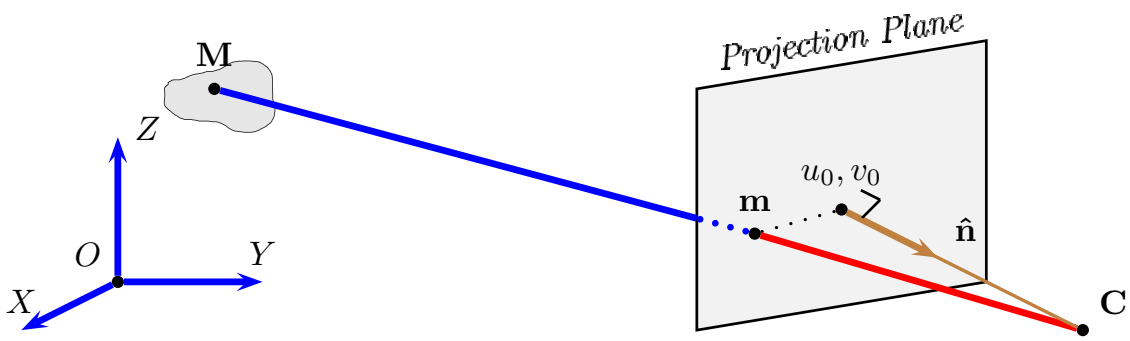

Figure 5.4: Illustrating the mapping from observed camera point **m** to 3D point **M**.

Using standard nomenclature (Zhang 2000), the mapped 2D point on image plane is defined as

$$\mathbf{m} = \begin{pmatrix} u \\ v \end{pmatrix} \tag{5.7}$$

with the 3D point on denoted by

$$\mathbf{M} = \begin{pmatrix} x \\ y \\ z \end{pmatrix} \tag{5.8}$$

It is conventional to then define augmented vectors

$$\widetilde{\mathbf{m}} = \begin{pmatrix} u \\ v \\ 1 \end{pmatrix} \tag{5.9}$$

and

$$\widetilde{\mathbf{M}} = \begin{pmatrix} x \\ y \\ z \\ 1 \end{pmatrix} \tag{5.10}$$

The image of $\mathbf{M}$ is $\mathbf{m}$. The projection of $\mathbf{m}$ from $\mathbf{M}$ is then assumed to be a linear translation, rotation and scaling defined by

$$s\widetilde{\mathbf{m}} = \mathbf{P}\widetilde{\mathbf{M}} \tag{5.11}$$

where s is an (arbitrary) scaling factor and $\mathbf{P}$ is the 3×4 projection matrix. $\mathbf{P}$ is further decomposed into a translation vector $\mathbf{t}$ and rotation matrix $\mathbf{R}$. The projection matrix also needs to represent the origin and scaling on the projection surface. Thus

$$\mathbf{P} = \mathbf{A}\,[\,\mathbf{R} \mid \mathbf{t}\,] \tag{5.12}$$

where $\mathbf{A}$ is

$$\mathbf{A} = \begin{pmatrix} \alpha & \gamma & u_o \\ 0 & \beta & v_o \\ 0 & 0 & 1 \end{pmatrix} \tag{5.13}$$

$\mathbf{R}$ and $\mathbf{t}$ are the so-called *extrinsic* parameters, the rotation and translation which relate the world co-ordinate system to the camera co-ordinate system (Zhang 2000). $\mathbf{A}$ is composed of the camera *intrinsic* parameters, comprising the co-ordinates of the plane's principal point (u_o, v_o), α and β scale factors in the u, v directions, and γ the skew of the image axes. $\mathbf{A}$ is thus also referred to as the *intrinsic matrix* (Zhang 2000). Essentially, what is left is $\mathbf{P}$, a 3×4 matrix of unknown parameters, however the intuitive interpretation of its decomposition into fundamental operations of rotation, translation, skewing and scaling is useful.

$\mathbf{P}$ needs to be estimated, and the derivation of results outlined in Section 2.3.2 of Medioni & Kang (2004). Given each 2D $\leftrightarrow$ 3D correspondence

$$\mathbf{m}_i = \begin{pmatrix} u_i \\ v_i \end{pmatrix} \leftrightarrow \mathbf{M}_i = \begin{pmatrix} x_i \\ y_i \\ z_i \end{pmatrix} \tag{5.14}$$

the development of the projective mapping equation can proceed. The projection matrix in terms of components is

$$\mathbf{P} = \begin{pmatrix} p_{11} & p_{12} & p_{13} & p_{14} \\ p_{21} & p_{22} & p_{23} & p_{24} \\ p_{31} & p_{32} & p_{33} & p_{34} \end{pmatrix} \tag{5.15}$$

thus

$$s \begin{pmatrix} u_i \\ v_i \\ 1 \end{pmatrix} = \begin{pmatrix} p_{11} & p_{12} & p_{13} & p_{14} \\ p_{21} & p_{22} & p_{23} & p_{24} \\ p_{31} & p_{32} & p_{33} & p_{34} \end{pmatrix} \begin{pmatrix} x_i \\ y_i \\ z_i \\ 1 \end{pmatrix} \tag{5.16}$$

Expanding, three equations can be written

$$s\,u_i = p_{11}x_i + p_{12}y_i + p_{13}z_i + p_{14} \tag{5.17}$$

$$s\,v_i = p_{21}x_i + p_{22}y_i + p_{23}z_i + p_{24} \tag{5.18}$$

$$s = p_{31}x_i + p_{32}y_i + p_{33}z_i + p_{34} \tag{5.19}$$

Multiplying (5.19) by u_i and subtracting from (5.17),

$$\begin{aligned} s\,u_i &= p_{11}x_i + p_{12}y_i + p_{13}z_i + p_{14} \\ - & \\ s, u_i &= p_{31}x_iu_i + p_{32}y_iu_i + p_{33}z_iu_i + p_{34}u_i \\ \rightarrow \quad 0 &= p_{11}x_i + p_{12}y_i + p_{13}z_i + p_{14} \\ & \quad -p_{31}x_iu_i - p_{32}y_iu_i - p_{33}z_iu_i - p_{34}u_i \end{aligned} \tag{5.20}$$

Similarly, multiplying (5.19) by v_i and subtracting from (5.18),

$$\begin{aligned} s\,v_i &= p_{21}x_i + p_{22}y_i + p_{23}z_i + p_{24} \\ - & \\ s, v_i &= p_{31}x_iv_i + p_{32}y_iv_i + p_{33}z_iv_i + p_{34}v_i \\ \rightarrow \quad 0 &= p_{21}x_i + p_{22}y_i + p_{23}z_i + p_{24} \\ & \quad -p_{31}x_iv_i - p_{32}y_iv_i - p_{33}z_iv_i - p_{34}v_i \end{aligned} \tag{5.21}$$

Writing equations (5.70) and (5.71) in matrix form

$$\begin{pmatrix} x_i\, y_i\, z_i\, 1 & 0 & 0 & 0\, 0 & -x_i u_i & -y_i u_i & -z_i u_i & -u_i \\ 0 & 0 & 0\, 0 & x_i\, y_i\, z_i\, 1 & -x_i v_i & -y_i v_i & -z_i v_i & -v_i \end{pmatrix} \begin{pmatrix} p_{11} \\ p_{12} \\ p_{13} \\ p_{14} \\ p_{21} \\ p_{22} \\ p_{23} \\ p_{24} \\ p_{31} \\ p_{32} \\ p_{33} \\ p_{34} \end{pmatrix}$$

$$= \begin{pmatrix} 0 \\ 0 \end{pmatrix} \tag{5.22}$$

which, for the purposes of solution, is more compactly expressed as

$$\mathbf{G}\,\mathbf{p} \;=\; \mathbf{0} \tag{5.23}$$

where $\mathbf{G}$ is the 2×12 matrix of known parameters, $\mathbf{p}$ is the 12×1 vector of coefficients of the $\mathbf{P}$ calibration matrix, and $\mathbf{0}$ is the 2×1 zero vector. Next, for a set of observations, $\mathbf{G}_i$ sets are all stacked together to yield

$$\begin{pmatrix} \text{———} & \mathbf{G}_1 & \text{———} \\ \text{———} & \mathbf{G}_1 & \text{———} \\ & \vdots & \\ \text{———} & \mathbf{G}_n & \text{———} \end{pmatrix} \begin{pmatrix} | \\ p_{ij} \\ | \end{pmatrix} = \begin{pmatrix} 0 \\ \vdots \\ 0 \end{pmatrix} \tag{5.24}$$

So the problem is to find

$$\min_{\mathbf{p}} \parallel \mathbf{Gp} \parallel^2 \tag{5.25}$$

This follows a standard solution (Anton 2003), since in general

$$\begin{aligned} \| \mathbf{Ax} \|^2 &= \mathbf{Ax} \cdot \mathbf{Ax} \\ &= \mathbf{x} \cdot \mathbf{A}^T \mathbf{Ax} \\ &= \mathbf{x} \cdot \lambda \mathbf{x} \\ &= \lambda \left(\mathbf{x} \cdot \mathbf{x} \right) \\ &= \lambda \| \mathbf{x} \|^2 \end{aligned} \tag{5.26}$$

Hence solving $\mathbf{Ax} \approx 0$ corresponds to finding the minimum eigenvalue λ of $\mathbf{A}^T\mathbf{A}$, and the solution is the corresponding eigenvector. Thus here there is $\mathbf{G}^T\mathbf{G}$, and the corresponding eigenvector is the estimate for $\mathbf{p}$, which is then reshaped into the matrix $\mathbf{P}$.

Recall now that the problem definition had

$$\mathbf{P} = \mathbf{A} \left[\mathbf{R} \mid \mathbf{t} \right] \tag{5.27}$$

where $\mathbf{A}$ is

$$\mathbf{A} = \begin{pmatrix} \alpha & \gamma & u_o \\ 0 & \beta & v_o \\ 0 & 0 & 1 \end{pmatrix} \tag{5.28}$$

Denote the 3×3 submatrix of $\mathbf{P}$ by $\mathbf{B}$, and the last column of $\mathbf{P}$ by $\mathbf{b}$. So

$$\mathbf{P} = \left(\mathbf{B} \mid \mathbf{b} \right) \tag{5.29}$$

Thus,

$$\mathbf{B} = \mathbf{AR} \tag{5.30}$$

$$\mathbf{b} = \mathbf{At} \tag{5.31}$$

So if $\mathbf{R}$ is an orthogonal matrix with unit norm,

$$\mathbf{B}^T = (\mathbf{AR})^T \tag{5.32}$$

$$= \mathbf{R}^T \mathbf{A}^T \tag{5.33}$$

and thus

$$\mathbf{B}\mathbf{B}^T = \mathbf{A}\mathbf{R}\mathbf{R}^T\mathbf{A}^T \tag{5.34}$$

$$= \mathbf{A}\mathbf{A}^T \tag{5.35}$$

With

$$\mathbf{K} = \mathbf{A}\mathbf{A}^T \tag{5.36}$$

$$= \mathbf{B}\mathbf{B}^T \tag{5.37}$$

multiplication of elements of $\mathbf{A}$,

$$\mathbf{K} = \mathbf{A}\mathbf{A}^T \tag{5.38}$$

$$= \begin{pmatrix} \alpha & \gamma & u_o \\ 0 & \beta & v_o \\ 0 & 0 & 1 \end{pmatrix} \begin{pmatrix} \alpha & 0 & 0 \\ \gamma & \beta & 0 \\ u_o & v_o & 1 \end{pmatrix} \tag{5.39}$$

$$= \begin{pmatrix} \alpha^2 + \gamma^2 + u_o^2 & \beta\gamma + u_o v_o & u_o \\ \beta\gamma + u_o v_o & \beta^2 + v_o^2 & v_o \\ u_o & v_o & 1 \end{pmatrix} \tag{5.40}$$

Thus the individual intrinsic parameters can be solved $\alpha, \beta, \gamma, u_o, v_o$. In practice, Zhang notes the possible need to normalize $\mathbf{K}$ such that $\mathbf{K}(3,3) = 1$. Then,

$$u_o = K(1,3) \tag{5.41}$$

$$u_o = K(3,1) \tag{5.42}$$

$$v_o = K(2,3) \tag{5.43}$$

$$v_o = K(3,2) \tag{5.44}$$

$$\beta = \sqrt{K(2,2) - v_o^2} \tag{5.45}$$

$$\gamma = \frac{K(2,1) - u_o v_o}{\beta} \tag{5.46}$$

$$\alpha = \sqrt{K(1,1) - \gamma^2 - u_o^2} \tag{5.47}$$

Finally the extrinsic parameters can be solved

$$\mathbf{R} = \mathbf{A}^{-1}\mathbf{B} \tag{5.48}$$

$$\mathbf{t} = \mathbf{A}^{-1}\mathbf{b} \tag{5.49}$$

R and **t** are the so-called *extrinsic* parameters, the rotation and translation which relate the world co-ordinate system to the camera co-ordinate system (Zhang 2000). In the following sections the formulation is extended to the 2-camera case. Extending the method to multiple cameras increases accuracy and reduces interruptions to connectivity. In an operating environment, it is important to keep constant connectivity to the needle and often there are unpredicted movements such as the surgeons hands blocking the camera during the procedure.

5.2.2 Mapping Algorithm to Multiple Cameras in 3D

The information from two infrared cameras may now be incorporated. Once **P** has been determined, given (u, v) can be mapped to (x, y, z). Clearly this requires more than one camera. Since (x, y, z) are unknown, as well as the scaling s, there are 4 unknowns. A similar re-organization of the equations is performed, as follows.

$$p_{11}x_i + p_{12}y_i + p_{13}z_i - su_i = -p_{14} \tag{5.50}$$

$$p_{21}x_i + p_{22}y_i + p_{23}z_i - sv_i = -p_{24} \tag{5.51}$$

$$p_{31}x_i + p_{32}y_i + p_{33}z_i - s = -p_{34} \tag{5.52}$$

into matrix form

$$\begin{pmatrix} p_{11} & p_{12} & p_{13} & -u_i \\ p_{21} & p_{22} & p_{23} & -v_i \\ p_{31} & p_{32} & p_{33} & -1 \end{pmatrix} \begin{pmatrix} x_i \\ y_i \\ z_i \\ s \end{pmatrix} = \begin{pmatrix} -p_{14} \\ -p_{24} \\ -p_{34} \end{pmatrix} \tag{5.53}$$

Now denote $p_{ij}^{(k)}$ as parameter p_{ij} for camera k. Thus for 2 cameras,

$$\begin{pmatrix} p_{11}^{(1)} & p_{12}^{(1)} & p_{13}^{(1)} & -u^{(1)} & 0 \\ p_{21}^{(1)} & p_{22}^{(1)} & p_{23}^{(1)} & -v^{(1)} & 0 \\ p_{31}^{(1)} & p_{32}^{(1)} & p_{33}^{(1)} & -1 & 0 \\ \hline p_{11}^{(2)} & p_{12}^{(2)} & p_{13}^{(2)} & 0 & -u^{(2)} \\ p_{21}^{(2)} & p_{22}^{(2)} & p_{23}^{(2)} & 0 & -v^{(2)} \\ p_{31}^{(2)} & p_{32}^{(2)} & p_{33}^{(2)} & 0 & -1 \end{pmatrix} \begin{pmatrix} x \\ y \\ z \\ s^{(1)} \\ s^{(2)} \end{pmatrix} \tag{5.54}$$

$$= \begin{pmatrix} -p_{14}^{(1)} \\ -p_{24}^{(1)} \\ -p_{34}^{(1)} \\ \hline -p_{14}^{(2)} \\ -p_{24}^{(2)} \\ -p_{34}^{(2)} \end{pmatrix} \tag{5.55}$$

which is of the form

$$\mathbf{Hr} = \mathbf{h} \tag{5.56}$$

This may be found using the Moore-Penrose pseudoinverse to give

$$\mathbf{r}^* = \left(\mathbf{H}^T\mathbf{H}\right)^{-1}\mathbf{H}^T\mathbf{h} \tag{5.57}$$

Finally, the components of $\mathbf{r}$ are the estimated position

$$\mathbf{r}^* = \begin{pmatrix} \hat{x} \\ \hat{y} \\ \hat{z} \end{pmatrix} \tag{5.58}$$

5.2.3 3D Experimental Results

To check the correctness of the algorithm as derived, a test stub was developed to project a set of random points through a plane representing each camera. The ray-plane intersection point was then as the (u, v) camera point, and the projection algorithm as described was used to estimate the true (x, y, z) point.

The combined system was then tested with real data from the two IR sensors where real-time data acquisition is able to translate to the estimated 3D position as the IR sources are moved as outlined in (Appendix C) and also depicted in Figure 5.5 and 5.6. The oulier data was caused by interference during the experiment such as the camera picking up an incorrect signal or at times hand movements blocking the camera.

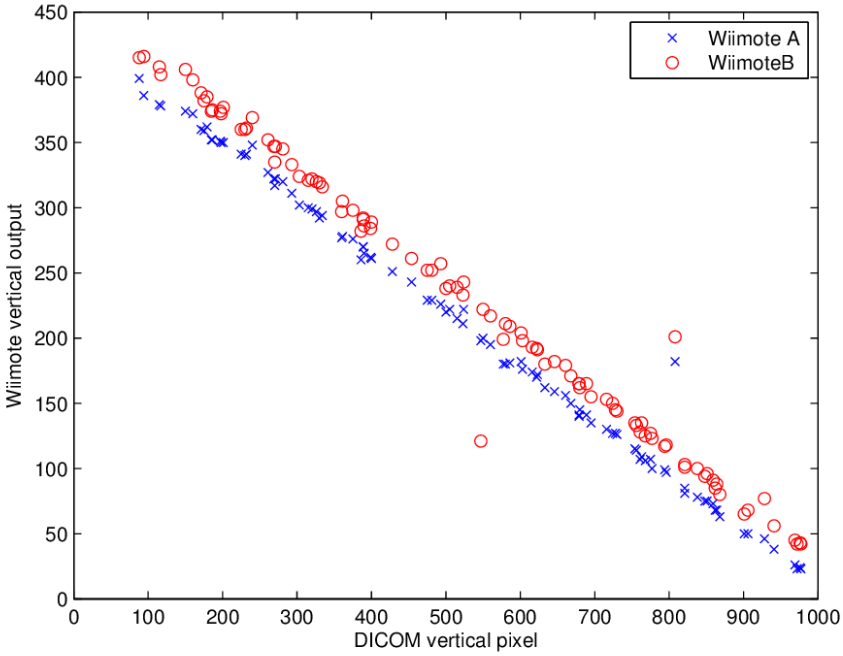

Figure 5.5: IR Camera output and the DICOM vertical pixels.

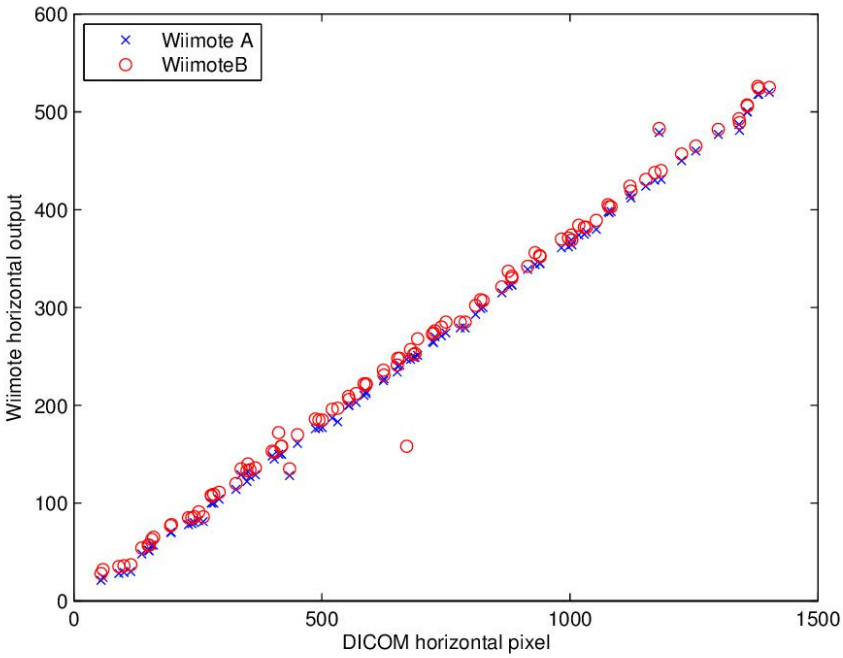

Figure 5.6: IR Camera output and the DICOM horizontal pixels.

5.3 Review of Clinical Trials

A review of the clinical results and the preference of the operators suggested that the 3D navigation system, although very interesting, was not focused on addressing the main issue which was advancing the needle towards the lesion of interest. The lack of spatial referencing in a biopsy scenario may be better addressed by a simpler display of the two 2D camera setup. The overwhelming majority of the operators also suggested advancing the system to two separate cameras in order to help with needle visibility. Therefore the system was further developed into two infrared cameras each as a 2D view demonstrated in the following section.

5.4 2x2D System

The clinical review of the 3D system highlighted the specifics around what clinicians require and expect when it comes to biopsy navigation systems. The review identified that the focus of the navigation system should be on the precise entry angle and assistance with spacial referencing as the needle is advanced towards the lesion of interest. Therefore in this chapter the 3D approach is extended to two cameras that detect the needle and project it onto a 2D plane, thus enabling the clinician to reference back and forth between the X-ray DICOM images and the navigation system interface.

5.4.1 Mapping Algorithm

The 2D approach would be to utilise the precise knowledge of the camera position, comprising its centre (u_0, v_0) and orientation with respect to the DICOM XY axes. Furthermore, the scaling with respect to the DICOM plane is required. In general, this information is not available; in our situation, it is impossible to acquire because it would require precise calibration of imaging centre points and camera orientations and it would also need the camera intrinsic and extrinsic parameters, i.e. focal length, angle of alignment.

The 2D point on the imaging plane is defined as

$$\mathbf{m} = \begin{pmatrix} u \\ v \end{pmatrix} \tag{5.59}$$

with the target 2D point on the mapped display denoted by

$$\mathbf{M} = \begin{pmatrix} x \\ y \end{pmatrix} \tag{5.60}$$

It is conventional to then define augmented vectors

$$\widetilde{\mathbf{m}} = \begin{pmatrix} u \\ v \\ 1 \end{pmatrix} \tag{5.61}$$

and

$$\widetilde{\mathbf{M}} = \begin{pmatrix} x \\ y \\ 1 \end{pmatrix} \tag{5.62}$$

The utility of this approach becomes evident when the mapping solution is solved. The projection of $\mathbf{M}$ is $\mathbf{m}$. The $\mathbf{M}$ is mapped to $\mathbf{m}$ for the image, and it is necessary to translate from measured $\mathbf{m}$ to estimated $\mathbf{M}$. This is assumed to be a linear translation, rotation and scaling defined by

$$s\widetilde{\mathbf{m}} = \mathbf{P}\widetilde{\mathbf{M}} \tag{5.63}$$

where s is an (arbitrary) scaling factor and $\mathbf{P}$ is the 3×3 projection matrix.

$\mathbf{P}$ will now need to be estimated given each 2D $\leftrightarrow$ 2D correspondence

$$\mathbf{m}_i = \begin{pmatrix} u_i \\ v_i \end{pmatrix} \leftrightarrow \mathbf{M}_i = \begin{pmatrix} x_i \\ y_i \end{pmatrix} \tag{5.64}$$

the projective mapping equation can now proceed to develop.

The projection matrix in terms of components is

$$\mathbf{P} = \begin{pmatrix} p_{11} & p_{12} & p_{13} \\ p_{21} & p_{22} & p_{23} \\ p_{31} & p_{32} & p_{33} \end{pmatrix} \tag{5.65}$$

thus

$$s \begin{pmatrix} u_i \\ v_i \\ 1 \end{pmatrix} = \begin{pmatrix} p_{11} & p_{12} & p_{13} \\ p_{21} & p_{22} & p_{23} \\ p_{31} & p_{32} & p_{33} \end{pmatrix} \begin{pmatrix} x_i \\ y_i \\ 1 \end{pmatrix} \tag{5.66}$$

Expanding, three equations can be written

$$s\,u_i = p_{11}x_i + p_{12}y_i + p_{13} \tag{5.67}$$

$$s\,v_i = p_{21}x_i + p_{22}y_i + p_{23} \tag{5.68}$$

$$s = p_{31}x_i + p_{32}y_i + p_{33} \tag{5.69}$$

Multiplying (5.69) by u_i and subtracting from (5.67),

$$\begin{aligned} s\,u_i &= p_{11}x_i + p_{12}y_i + p_{13} \\ - & \\ s, u_i &= p_{31}x_iu_i + p_{32}y_iu_i + p_{33}u_i \\ \rightarrow \quad 0 &= p_{11}x_i + p_{12}y_i + p_{13} \\ & \qquad -p_{31}x_iu_i - p_{32}y_iu_i - p_{33}u_i \end{aligned} \tag{5.70}$$

Similarly, multiplying (5.69) by v_i and subtracting from (5.68),

$$\begin{aligned} s\,v_i &= p_{21}x_i + p_{22}y_i + p_{23} \\ - & \\ s, v_i &= p_{31}x_iv_i + p_{32}y_iv_i + p_{33}v_i \\ \rightarrow \quad 0 &= p_{21}x_i + p_{22}y_i + p_{23} \\ & \qquad -p_{31}x_iv_i - p_{32}y_iv_i - p_{33}v_i \end{aligned} \tag{5.71}$$

Writing equations (5.70) and (5.71) in matrix form, there is

$$\begin{pmatrix} x_i\, y_i\, 1 & 0 & 0\, 0 & -x_i u_i & -y_i u_i & -u_i \\ 0 & 0\, 0\, x_i & y_i\, 1 & -x_i v_i & -y_i v_i & -v_i \end{pmatrix} \begin{pmatrix} p_{11} \\ p_{12} \\ p_{13} \\ p_{21} \\ p_{22} \\ p_{23} \\ p_{31} \\ p_{32} \\ p_{33} \end{pmatrix} = \begin{pmatrix} 0 \\ 0 \end{pmatrix}$$

which, for the purposes of solution, is more compactly expressed as

$$\mathbf{G}\,\mathbf{p} \;=\; \mathbf{0} \tag{5.72}$$

where $\mathbf{G}$ is the 2×9 matrix of known parameters, $\mathbf{p}$ is the 9×1 vector of coefficients of the $\mathbf{P}$ calibration matrix, and $\mathbf{0}$ is the 2×1 zero vector. Next, for a set of observations, $\mathbf{G}_i$ sets are stacked together to yield

$$\begin{pmatrix} \text{———} & \mathbf{G}_1 & \text{———} \\ \text{———} & \mathbf{G}_1 & \text{———} \\ & \vdots & \\ \text{———} & \mathbf{G}_n & \text{———} \end{pmatrix} \begin{pmatrix} | \\ \\ p_{ij} \\ \\ | \end{pmatrix} = \begin{pmatrix} 0 \\ \vdots \\ 0 \end{pmatrix} \tag{5.73}$$

So the problem is to find

$$\min_{\mathbf{p}} \parallel \mathbf{Gp} \parallel^2 \tag{5.74}$$

This follows a standard solution (Anton 2003), since in general

$$\begin{aligned} \parallel \mathbf{Ax} \parallel^2 &= \mathbf{Ax} \cdot \mathbf{Ax} \\ &= \mathbf{x} \cdot \mathbf{A}^T \mathbf{Ax} \\ &= \mathbf{x} \cdot \lambda \mathbf{x} \\ &= \lambda\, (\mathbf{x} \cdot \mathbf{x}) \\ &= \lambda \parallel \mathbf{x} \parallel^2 \end{aligned} \tag{5.75}$$

Hence solving $\mathbf{Ax} \approx 0$ corresponds to finding the minimum eigenvalue λ of $\mathbf{A}^T\mathbf{A}$, and the solution is the corresponding eigenvector. Thus there is $\mathbf{G}^T\mathbf{G}$, and the corresponding eigenvector is the estimate for $\mathbf{p}$, which is then reshaped into the matrix $\mathbf{P}$.

In the following, this approach is extended to the 2-camera case in order to take advantage of more than one viewpoint and this can provide greater accuracy.

5.4.2 Mapping Algorithm to Multiple Cameras in 2D

Once **P** has been determined, (u, v) can be mapped into (x, y). There will, however, be error in any measurements taken and this will result in errors in the estimated positions. The errors can be reduced by using multiple cameras, then finding the estimated position which best matches all observations.

A similar re-organisation of the equations is performed, as follows.

$$p_{11}x_i + p_{12}y_i - su_i = -p_{13} \tag{5.76}$$

$$p_{21}x_i + p_{22}y_i - sv_i = -p_{23} \tag{5.77}$$

$$p_{31}x_i + p_{32}y_i - s = -p_{33} \tag{5.78}$$

into matrix form

$$\begin{pmatrix} p_{11} & p_{12} & -u_i \\ p_{21} & p_{22} & -v_i \\ p_{31} & p_{32} & -1 \end{pmatrix} \begin{pmatrix} x_i \\ y_i \\ s \end{pmatrix} = \begin{pmatrix} -p_{13} \\ -p_{23} \\ -p_{33} \end{pmatrix} \tag{5.79}$$

Now denote $p_{ij}^{(k)}$ as parameter p_{ij} for camera k. Thus for 2 cameras,

$$\left(\begin{array}{cccc} p_{11}^{(1)} & p_{12}^{(1)} & -u^{(1)} & 0 \\ p_{21}^{(1)} & p_{22}^{(1)} & -v^{(1)} & 0 \\ p_{31}^{(1)} & p_{32}^{(1)} & -1 & 0 \\ \hline p_{11}^{(2)} & p_{12}^{(2)} & 0 & -u^{(2)} \\ p_{21}^{(2)} & p_{22}^{(2)} & 0 & -v^{(2)} \\ p_{31}^{(2)} & p_{32}^{(2)} & 0 & -1 \end{array}\right) \begin{pmatrix} x \\ y \\ s^{(1)} \\ s^{(2)} \end{pmatrix} \tag{5.80}$$

$$= \begin{pmatrix} -p_{13}^{(1)} \\ -p_{23}^{(1)} \\ -p_{33}^{(1)} \\ \hline -p_{13}^{(2)} \\ -p_{23}^{(2)} \\ -p_{33}^{(2)} \end{pmatrix} \tag{5.81}$$

which is of the form

$$\mathbf{Hr} = \mathbf{h} \tag{5.82}$$

Since $\mathbf{H}$ is not square, it cannot be inverted in the conventional sense to find $\mathbf{r}$. In most cases there will be no value for $\mathbf{r}$ so that the equation is exactly true, so a value of $\mathbf{r}$ is chosen that makes the equation closest to being true. In this case, $\mathbf{H}$ is an overdetermined matrix, and the aim is to compute $\mathbf{r}$ so that the squared error between $\mathbf{Hr}$ and $\mathbf{h}$ is minimized. It is required to find vector $\mathbf{r}^* = \min_{\mathbf{r}} ||\mathbf{Hr} - \mathbf{h}||_2$. This may be found using the Moore-Penrose pseudoinverse to give

$$\mathbf{r}^* = \left(\mathbf{H}^T\mathbf{H}\right)^{-1}\mathbf{H}^T\mathbf{h} \tag{5.83}$$

Finally, the components of $\mathbf{r}^*$ are the estimated position

$$\mathbf{r}^* = \begin{pmatrix} \hat{x} \\ \hat{y} \end{pmatrix} \tag{5.84}$$

This value $\mathbf{r}^*$ is the location of the needle endpoint on the DICOM image which is the aim of the algorithm presented here. The next section demonstrates the experimental results using the algorithm defined above.

5.4.3 2x2D Experimental Results

To test the model, two infrared cameras were set up to record the locations of a needle tip. The location of the needle tip is also measured using X-ray imaging and the position read from the DICOM image. The DICOM image provides the 2D target location (x, y),

while the pixel locations measured from the infrared camera provides the training data. This was done for 100 needle point positions, with DICOM images and infrared camera locations recorded for each position. To measure the effectiveness of this approach, we use leave-one-out cross-validation. This involves using 99 points to train the model, then testing it on the 100th point. The predicted location can then be compared to the actual measured location. This is repeated for every sample (100 times). By doing it this way it can be ensured that no training information is ever used for testing, as this would give unrealistically good results.

The measurement technique proposed requires knowledge of the needle positions. The needle positions are measured using infrared cameras which must be interfaced with a laptop and two separate infrared reflective tapes attached to the biopsy needle. The reflective point separation is 200mm and is estimated to be 204mm as shown in Figure 5.7 and outlined in (Appendix C). The infrared reflective tape was found to be an effective method for locating the needle using the infrared camera. The length of the needle is also required to extrapolate the actual endpoint of the needle.

The DICOM image is 512 by 512 pixels, with 2.048 pixels corresponding to 1mm. This was found by placing an object with known dimensions into the scanning area and measuring its size in the image. This allows the conversion of pixel based measurements to real distances by dividing errors measured in pixels by 2.048.

The error for the ith measurement is computed as:

$$E_i = \sqrt{(x_p - x_a)^2 + (y_p - y_a)^2} \tag{5.85}$$

where x_p and y_p are the predicted x, y locations and x_a and y_a are the actual or measured locations. This is the Euclidean distance between the measured and predicted points: high errors mean our prediction was very poor. The final average error is simply the mean of all the individual errors over the 100 points:

$$\bar{E} = \frac{1}{N}\sum_{1}^{N} E_i \tag{5.86}$$

For artificial data, it is possible to achieve errors very close to 0 (i.e. basically no error in prediction) since there is no noise. Once experiments are actually performed though, noise is introduced because the measured locations would not exactly match the real locations.

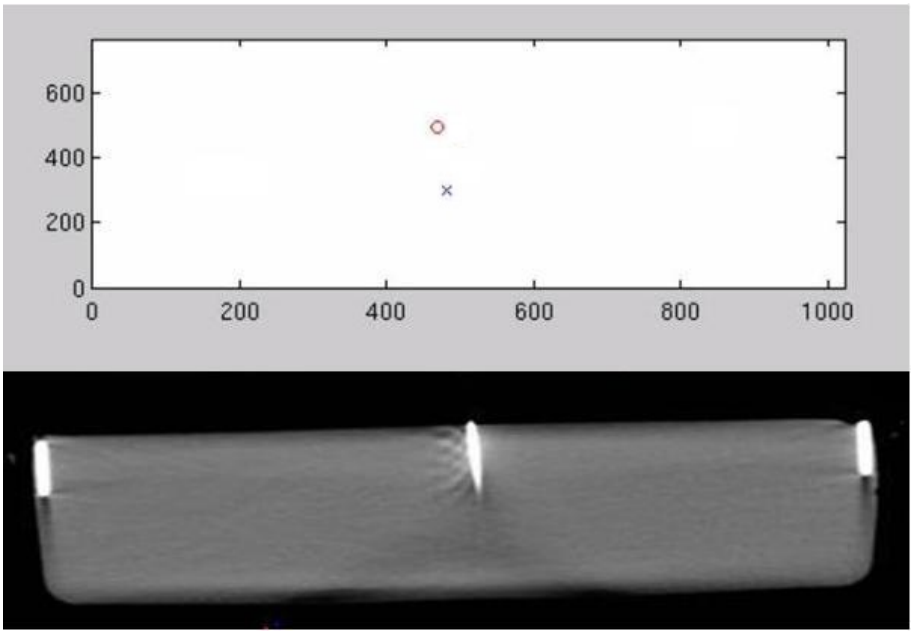

Figure 5.7: Location of the needle tip identified using two infrared cameras and also using the DICOM images. In the top image the 'x' and the 'o' are live outputs from the IR cameras and demonstrate the location of the needle using the reflection from two infrared reflective tapes. The dimensions of the top image are the raw locations from the IR camera, they are converted to an actual location using the method proposed in this research. The measurement scales are in millimeters.

Once the error is estimated for each point, a histogram can be plotted as shown in Figure 5.8. The mean error $\bar{E}$ across all points was 4.12 pixels (2.01mm), with a median of 3.89 pixels. This means that when predicting the location of a point on the DICOM image, the true location will be within ∼2mm of the predicted location. If a circle is drawn with a radius of 2mm on the DICOM image, the true point will be inside it 50 percent of the time. With a circle of radius 4.15mm, the true point will be inside it 90% of the time.

This error has two main sources: modelling error and noise. Modelling error comes from non-linear effects which may be introduced by such as the camera lens, the algorithm presented above does not model camera distortion. Noise comes from a mismatch between the measured and actual locations of the training points. Noise introduced in this way will increase the error when point locations are later estimated. Methods for camera calibration based on tracking image features while the camera undergoes rotation has previously been investigated by (Stein 1995) who demonstrated that lens distortion error can be reduced significantly.

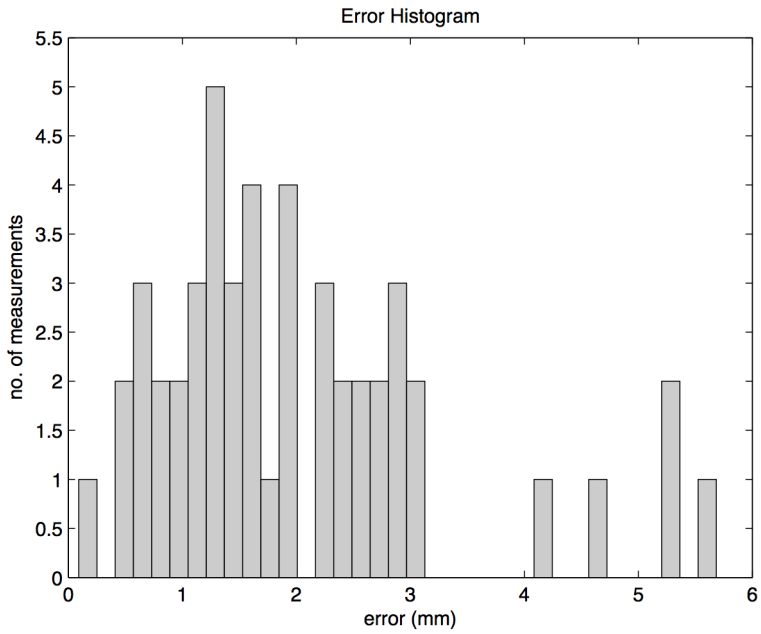

Figure 5.8: Error histogram showing the error from each of the 100 measurements, demonstrating that the error for half the measurements is less than ∼2mm, with a maximum error of 5.5mm. This error represents Euclidean distance between the true position and estimated position on the DICOM image.

5.5 Chapter Summary

The problem of radiation dosage in CT-assisted scans is the main focus of this research and this chapter introduced a solution which involves infrared camera pair, infrared emitter attached to the biopsy needle and custom written software to estimate the true biopsy needle position. Various tests were conducted which indicate that the infrared algorithm has the potential to achieve more accurate results compared to freehand (Appendix B). It is anticipated that occlusion of the needle will occur in real-life situations, and this also suggests that the use of multiple cameras will be essential. The mapping problem was shown to be able to be solved using a linear estimator, and the inverse (prediction) problem produced stable numerical results. The clinicians who operated the system were overwhelmingly in favor of a simple navigation system that assisted them with the lack of spatial referencing. When presented with a more complex 3D version of the system, it was identified that the simpler 2D system is more appropriate for their purpose.

Chapter 6

Clinical Performance Evaluation

In this chapter the clinical performance of the navigation system was tested in a controlled training environment using a phantom and scenarios resembling real-life biopsy procedures. The training module was configured and evaluated at the Princess Alexandra Hospital in Brisbane and radiologists undertaking competency-based training were requested to practice biopsy scenarios using the setup described in (Appendix D). The experience of the staff who used the system is documented in a survey results in (Appendix H). The scenarios and biopsy setup were designed and implemented with close consultations with senior Radiologists. The experimental results were analysed as in-plane needle targeting error and depth error. The targeting accuracy was calculated by finding the distance between the actual needle and the intended target location in CT coordinates. The actual needle location was recorded as the center of the signal void visible in the needle verification images. The needle depth error was measured as the number of 3 mm slices between the actual needle tip and the depth calculated by the CT scanner targeting software.

6.1 Biopsy Scenario Planning

Analysis of the clinical performance of the navigation system in Chapter 3 identified a number of issues regarding biopsy targeting. Specifically, the angle of entry and the

magnitude of the depth error, the small posterior and larger inferior systematic bias, the user errors in needle insertion, and the time required for repeated X-ray acquisition and correcting the trajectory were identified as problems that may benefit from technical improvements of biopsy guidance system. Consequently, there was an evident need to investigate alternative navigation techniques capable of addressing the issues identified with the navigation system. To that end several registration techniques and motifs of fiducial markers were examined. In particular the objective was to investigate methods that would improve the entry and depth error as well as eliminate user errors and reduce X-ray time through automated techniques.

For the purposes of this study, a series of common chest, pelvis and abdominal biopsy scenarios were constructed with the help of senior Radiologists at the Princess Alexandra Hospital in Brisbane. These scenarios included lung, renal, abdomen biopsies and percutaneous biopsy of spinal lesions.

6.2 User Experience and Survey

The infrared guided biopsy needle system was tested and evaluated by multiple radiologists, clinicians and radiographers. Overall more than 45 operators used the system and participated in the survey (Appendix G). The most common feedback from the survey was that the system is very helpful in addressing the lack of spatial referencing during a biopsy procedure particularly with the angle of entry of the needle. Using the system, the operator is able to use the information that is compellingly direct and intuitive and as such can plan the biopsy procedure more efficiently and accurately. The analysis of the results of the survey provided a comprehensive understanding of what a clinician expects. Some shortcomings of the system were also identified, most of which can be addressed by the further integration of the system into CT scanners as discussed in Section 7.2.

Using the top box method, the percentage of people who answered the most positive option were 91.

The clinicians who operated the system were presented with the following questions:

1. Is the system easy to use;
2. Does the system help with spatial referencing;
3. Is it a useful educational tool;
4. Is the system fast enough;
5. Does the system detect the needle properly;
6. Can the needle be sterilised easily;
7. Does the IR tape have a negative impact on trajectory;
8. Does the system reduce the number of repeated CT scans;
9. Is the system disruptive during the biopsy procedure;
10. How would you rate the system interface (GUI);
11. Should the system be integrated with the CT scanner;
12. Should the system be used in real life patient trials;
13. Does the system save time and reduce radiation in biopsy procedures;

According to the survey, features that made this system particularly suited for medical applications and in particular biopsy procedures included:

1. Ease of use;
2. Helps with spatial referencing;
3. Usefulness for educating junior clinicians;
4. Detecting the needle effectively;
5. Effective sterilisation of the needle with the infrared tape attached;
6. Reduction of the number of required scans;

Figure 6.1: Survey Results - Undertaken by 45 operators of the system who then ranked the system in a series of 13 questions.

7. Simple and easy to understand user interface;

According to the survey features that made the system not so suitable for medical applications included:

1. The infrared tape sometimes gets blocked by hand movements;
2. The system needs to be integrated into the CT scanner;

6.3 Chapter Summary

The results of the survey which was completed by 45 trained radiologists who perform biopsy procedures on a regular basis clearly identifies the advantages of having an infrared navigation system during a biopsy procedure. Ease of use and help with spatial referencing were identified as some of the most usefull attributes of the system. There were also some concerns raised and it was suggested that the system will need to be integrated into the CT scanner and that hand movements during the procedure at times block the connection to the camera.

Chapter 7

Conclusions and Further Work

7.1 Conclusions

The research presented in this thesis aimed to develop a navigation system suitable for performing CT guided biopsy procedures. With this aim, the main objectives were identified to be the lack of spatial referencing during a biopsy procedure and the development of a training module where clinicians could trial biopsy scenarios. The problem of radiation dosage in CT-assisted scans was described, and a possible solution using an infrared camera pair to estimate the true biopsy needle position was proposed, tested and evaluated.

An existing approach was used and subsequently extended to help guide clinicians in advancing the biopsy needle during the procedure. This extended algorithm computed a scaled estimate of the needle endpoint and assists with navigating the biopsy needle through a dedicated and custom built graphical user interface. As a result a prototype training module was designed and built where clinicians could practice different entry angles and biopsy scenarios and as such help increase their spatial referencing.

Various experiments and different scenarios were designed and tested to demonstrate the correctness of the algorithm and provide real-life simulated scenarios where the operators had a chance to practice different entry angles and familiarise themselves with the equipment. Different tests were conducted and results demonstrated that the method is

robust and fast enough to be adapted for real-time clinical applications. A comprehensive survey was also undertaken by clinicians who used the system in order to highlight the advantages and disadvantages of the system and identify future enhancements.

Several vulnerabilities with the system hardware, software and registration methodology were discovered during analysis and corrective measures were taken to improve clinical performance. An ongoing development for the navigation system includes its integration into the CT scanner and also using more than two infrared cameras to maximise camera to needle connectivity.

7.2 Further Work

The achievements of this thesis provide not only contributions to the CT field but also provide a guide for future investigations. The major suggestions for future research are outlined below.

A significant improvement to the navigation would be to introduce intra-operative target tracking. This would involve tracking the lesion of interest also, while the needle is being advanced through the patient's body, without having to stop and repeat X-ray scans. This would not only reduce radiation and make the procedure faster and more accurate, but it would also make patient movements during a biopsy procedure such as breathing, not as detrimental to needle trajectory.

To further increase the positioning accuracy and also to ensure constant feedback from the needle, the use of more than two cameras is ideal. The algorithm has been demonstrated to achieve this in a realistic setting. It is anticipated that occlusion of the needle will occur in real-life situations, and this also suggests that the use of more than 2 cameras will be useful.

The navigation system was tested at a pre-clinical level. Additional issues are expected to arise in trials with patients, which did not arise in phantom trails. Pre-clinical trials were performed using anatomical models made of soft materials, while in a clinical case, with real patients, the actual properties of the real tissues may cause a deviation of the

needle from the expected trajectory. This is an important issue which needs further investigation.

There are many other procedures that would potentially benefit from the work presented in this thesis. While the graphical user interface was specific for the application, the tracking method, owing to its safety and flexibility, may be employed for accurate and fast instrument tracking in other delicate procedures such as ablations.

As identified by the clinicians survey in Section 6.2 and (Appendix G), by further developing this navigation system and integrating it with the CT scanner technology the system will be much more accessible and easier to use. It is important to note that the involvement of a major health-care provider is essential for the progression of the ideas and methods that have been proposed in this research. There is much work to be done before the system can be used on real patients and in real biopsy scenarios including testing and complete integration into the CT scanners. This can only be achieved with the involvement of a large health care provider who has the capacity to obtain the legal approvals for real patient biopsy trials and eventual implementation and integration into CT scanners and radiology best practices.

References

Adam, A. et al. (2014), *Grainger & Allison's Diagnostic Radiology*, Elsevier Health Sciences.

Albiol, F. et al. (2016), 'Geometrical calibration of x-ray imaging with rgb cameras for 3d reconstruction'.

Amis, E. S. (2007), 'American college of radiology white paper on radiation dose in medicine', *Journal of the american college of radiology* .

Anton, H. (2003), 'Contemporary linear algebra, maple technology resource manual'.

Appelbaum, L. et al. (2011), 'Electromagnetic navigation system for ct-guided biopsy of small lesions', *American Journal of Roentgenology* **196**(5), 1194–1200.

Arnolli, M. et al. (2015), 'An overview of systems for CT-and MRI-guided percutaneous needle placement in the thorax and abdomen', *The International Journal of Medical Robotics and Computer Assisted Surgery* .

Auricchio, F. et al. (2014), 'A simple framework to generate 3d patient-specific model of coronary artery bifurcation from single-plane angiographic images', *Computers in biology and medicine* **44**, 97–109.

Babapour, H. et al. (2016), 'Self-calibration of digital aerial camera using combined orthogonal models', *ISPRS Journal of Photogrammetry and Remote Sensing* **117**, 29–39.

Bairstow, P. J. et al. (2010), 'Reducing inappropriate diagnostic practice through education and decision support', *International Journal for Quality in Health Care* .

Baker, L. et al. (2008), 'Expanded use of imaging technology and the challenge of measuring value', *Health Affairs* **27**(6).

Barnard, S. et al. (1982), 'Computational stereo', *ACM Computing Surveys (CSUR)* **14**(4), 553–572.

Beckmann, E. C. (2014), 'Ct scanning the early days', *The British journal of radiology* .

Beir, V. (2006), 'Health risks from exposure to low levels of ionizing radiation', *BEIR VII phase* **2**.

Bindman, S. (2009), 'Radiation dose associated with common computed tomography examinations and the associated lifetime attributable risk of cancer', *Archives of Internal Medicine* **169**(22), 2078–2086.

Brenner, D. et al. (2007), 'Computed tomographyan increasing source of radiation exposure', *New England Journal of Medicine* **357**(22), 2277–2284.

Brouwer, O. (2012), 'Image navigation as a means to expand the boundaries of fluorescence-guided surgery', *Physics in medicine and biology* **57**.

Burdette, E. et al. (2003), 'Method and apparatus for spatial registration and mapping of a biopsy needle during a tissue biopsy'.

Busse, H. et al. (2007), 'Method for automatic localization of mr-visible markers using morphological image processing and conventional pulse sequences: Feasibility for image-guided procedures', *Journal of Magnetic Resonance Imaging* **26**(4).

Buysse, S. et al. (2016), 'Ablation needle guide'. US Patent 9,271,796.

Cerci, J. et al. (2016), 18f-fdg pet/ct-guided biopsy: Technical procedure, *in* 'Oncological PET/CT with Histological Confirmation', Springer, pp. 9–31.

Cham, M. D., Lane, M. E., Henschke, C. I. & Yankelevitz, D. F. (2008), Lung biopsy: special techniques, *in* 'Seminars in respiratory and critical care medicine', Vol. 29, Thieme Medical Publishers, pp. 335–349.

Chong, A. K. (2009), 'New developments in medical photogrammetry', *Geoinf Sci J* **9**(1), 41–50.

Choo, J. Y. et al. (2013), 'Percutaneous transthoracic needle biopsy of small (1 cm) lung nodules under c-arm cone-beam CT virtual navigation guidance', *European radiology* **23**.

Cleary, K. et al. (2002), 'Technology improvements for image-guided and minimally invasive spine procedures', *IEEE Transactions on Information Technology in Biomedicine* **6**(4), 249–261.

Commission, I. E. et al. (2002), *Medical electrical equipment-Part 2-33: Particular requirements for the safety of magnetic resonance equipment for medical diagnosis*, International Electrotechnical Commission.

Dalvi, N. P. (2014), 'Tracheal tubes', *Understanding Anesthetic Equipment & Procedures: A Practical Approach* p. 161.

Das, M. et al. (2006), 'Augmented reality visualization for CT guided interventions: System description, feasibility, and initial evaluation in an abdominal phantom', *Radiology* **240**(1), 230–235.

De Looper, M. et al. (2009), 'Measuring disparities in health status and in access and use of health care in oecd countries'.

De Vito, L. et al. (2014), 'Measurements and sensors for motion tracking in motor rehabilitation', *Instrumentation Measurement Magazine, IEEE* .

Delmas, C. et al. (2015), Three-dimensional curvilinear device reconstruction from two fluoroscopic views, *in* 'SPIE Medical Imaging', International Society for Optics and Photonics, pp. 94150F–94150F.

Demharter, J. et al. (2001), 'Percutaneous core-needle biopsy of enlarged lymph nodes in the diagnosis and subclassification of malignant lymphomas', *European radiology* **11**(2), 276–283.

Dempsey, J. F. (2014), 'System and method for image guidance during medical procedures'. US Patent 8,812,077.

Dimmick, S. et al. (2007), 'CT-guided procedures: evaluation of a phantom system to teach accurate needle placement', *Clinical Radiology* **62**.

Ding, J. et al. (2008), 'Accuracy analysis of an image-guided system for vertebroplasty spinal therapy based on electromagnetic tracking of instruments', *SPIE Medical Imaging* **6918**.

Ding, M. et al. (2003), 'A real-time biopsy needle segmentation technique using hough transform', *Medical physics* .

Duda, R. et al. (2012), *Pattern classification*, John Wiley & Sons.

Eggers, P. E. et al. (2015), 'Method, apparatus and system for complete examination of tissue with hand-held imaging devices having mounted cameras'. US Patent 20,150,366,535.

Einstein, A. J. et al. (2007), 'Radiation dose to patients from cardiac diagnostic imaging', *Circulation* **116**(11), 1290–1305.

Elhawary, H. et al. (2010), 'Robotic system for transrectal biopsy of the prostate: Real-time guidance under mri', *Engineering in Medicine and Biology Magazine, IEEE* **29**(2), 78–86.

Enquobahrie, A. et al. (2008), 'Designing tracking software for image-guided surgery applications: Igstk experience', *International journal of computer assisted radiology and surgery* .

Fischer, J., Battuello, M., Sadli, M., Ballico, M., Park, S., Saunders, P., Zundong, Y., Johnson, B. C., van der Ham, E., Li, W. et al. (2014), 'Cct-wg5 on radiation thermometry,uncertainty budgets for realisation of scales by radiation thermometry(bureau international des poids et mesures-bipm, sèvres, france, 2003)'.

Fixova, K. et al. (2014), In-hospital navigation system for people with limited orientation, *in* 'Cognitive Infocommunications (CogInfoCom), 2014 5th IEEE Conference on', IEEE, pp. 125–130.

Frederiksen, J. et al. (2015), 'Systematic review of the effectiveness of fine-needle aspiration and/or core needle biopsy for subclassifying lymphoma', **139**(2), 245–251.

Fuangrod, T. et al. (2016), 'Investigation of a real-time epid-based patient dose monitoring safety system using site-specific control limits', *Radiation Oncology* **11**(1), 106.

Galluzzo, A. et al. (2015), 'Current role of computed tomography-guided transthoracic needle biopsy of metastatic lung lesions', *Future Oncology* **11**(2s), 43–46.

Gneeniss, A. et al. (2015), 'In-flight photogrammetric camera calibration and validation via complementary lidar', *Journal of Photogrammetry and Remote Sensing* **100**, 3 – 13.

Golding, S. J. (2002), 'Radiation dose in CT: are we meeting the challenge?', *The British Journal of Radiology* **75**(889), 1–4.

Graham, R. et al. (2005), 'Dicom demystified: A review of digital file formats and their use in radiological practice', *Clinical Radiology* **60**(11), 1133 – 1140.

Grasso, R. F. et al. (2013), 'Percutaneous lung biopsies: performance of an optical CT-based navigation system with a low-dose protocol', *European radiology* **23**.

Groetz, S. et al. (2015), 'A new robotic assistance system for percutaneous CT-guided punctures: Initial experience', *Minimally Invasive Therapy & Allied Technologies* pp. 1–7.

Gruber-Rouh, T. et al. (2015*a*), 'Intervention planning using a laser navigation system for ct-guided interventions: a phantom and patient study', *Korean journal of radiology* **16**(4), 729–735.

Gruber-Rouh, T. et al. (2015*b*), 'Intervention planning using a laser navigation system for ct-guided interventions: a phantom and patient study', *Korean journal of radiology* **16**(4), 729–735.

Guimaraes, A. C. et al. (2003), 'Computed tomography-guided needle biopsies in pediatric oncology', *Journal of pediatric surgery* **38**(7), 1066–1068.

Gupta, R. K. et al. (2011), Accuracy Analysis of Kinect Depth Data, Calgary, Canada.

Hall, E. J. et al. (2008), 'Cancer risks from diagnostic radiology', *The British Journal of Radiology* **81**(965), 362–378.

Hallert, K. (1965), 'Photogrammetry in medicine', *Photogrammetria* **20**(2), 81–88.

Han, J. et al. (2013), 'Enhanced computer vision with microsoft kinect sensor: A review', *IEEE transactions on cybernetics* **43**(5), 1318–1334.

Hartley, R. et al. (2005), 'Multiple view geometry in computer vision', *Robotica* **23**(2), 271–271.

Hassard, M. et al. (2003), 'Training module to teach ultrasound-guided breast biopsy skills to residents improves accuracy', *Canadian Association of Radiologists Journal* **54**(3), 155.

Heike, C. L., Upson, K., Stuhaug, E. & Weinberg, S. M. (2010), '3d digital stereophotogrammetry: a practical guide to facial image acquisition', *Head & Face Medicine* .

Herman, G. T. (2009), *Fundamentals of Computerized Tomography: Image Reconstruction from Projections*, 2nd edn, Springer Publishing Company, Incorporated.

Housden, R. J. et al. (2013), 'Extended-field-of-view three-dimensional transesophageal echocardiography using image-based x-ray probe tracking', *Ultrasound in medicine & biology* **39**(6), 993–1005.

Hsieh, J. (2009), *Computed tomography: principles, design, artifacts, and recent advances.*

Jiang, H., et al. (2000), 'A localization algorithm and error analysis for stereo x-ray image guidance', *Medical physics* **27**(5), 885–893.

Jones, B. (1998), 'A reappraisal of the use of infrared thermal image analysis in medicine', *Medical Imaging, IEEE Transactions on* **17**(6), 1019–1027.

Kim, E. et al. (2014), 'CT-guided liver biopsy with electromagnetic tracking: Results from a single-center prospective randomized controlled trial', *American Journal of Roentgenology* **203**(6), W715–W723.

Kim, Y. et al. (2015), 'A portable and remote 6-dof pose sensor system with a long measurement range based on 1-d laser sensors', *Industrial Electronics, IEEE Transactions on* **62**(9).

Koninklijke-Philips-N.V. (2015), 'Computed tomography system. international patent ep2861149'.
URL: *https://worldwide.espacenet.com/*

Koyama, S. et al. (2013), A 3d vision 2.1 mpixel image sensor for single-lens camera systems, *in* '2013 IEEE International Solid-State Circuits Conference Digest of Technical Papers', IEEE, pp. 492–493.

Kreyszig, E. (2010), *Advanced engineering mathematics*, John Wiley & Sons.

Lal, H. et al. (2012), 'CT-guided percutaneous biopsy of intrathoracic lesions', *Korean journal of radiology* **13**(2), 210–226.

Lee, J. C. (2008), 'Hacking the nintendo wii remote', *IEEE pervasive computing* **7**(3), 39–45.

Lee., S. L. & others. (2010), 'From medical images to minimally invasive intervention: Computer assistance for robotic surgery', *Computerized Medical Imaging and Graphics* **34**(1), 33 – 45.

Leis, J. et al. (2012), Infrared camera imaging algorithm to augment CT-assisted biopsy procedures, *in* 'Signal Processing and Communication Systems (ICSPCS), 2012 6th International Conference on', IEEE, pp. 1–6.

Leong, S. et al. (2012), 'Electromagnetic navigation bronchoscopy: A descriptive analysis', *Journal of Thoracic Disease* **4**(2).

Lim, J. et al. (2015), '3-D cameras: A novel method and device for 3-D imaging using light detection and ranging', *Industrial Electronics Magazine, IEEE* **9**.

Livatino, S. et al. (2015), 'Stereoscopic visualization and 3-D technologies in medical endoscopic teleoperation', *Industrial Electronics, IEEE Transactions on* **62**(1).

Lloyd, G. et al. (2010), 'Gas plasma: medical uses and developments in wound care', *Plasma Processes and Polymers* **7**(3-4), 194–211.

Longuet-Higgins, H. C. (1987), 'A computer algorithm for reconstructing a scene from two projections', *Readings in Computer Vision: Issues, Problems, Principles, and Paradigms, MA Fischler and O. Firschein, eds* pp. 61–62.

Macnab, A. et al. (2012), 'Biomedical applications of wireless continuous wave near infrared spectroscopy', *Biomedical Spectroscopy and Imaging* **1**(3), 205–222.

Markwardt, N. A., Stepp, H., Franz, G., Sroka, R., Goetz, M., Zelenkov, P. & Rühm, A. (2016), 'Remission spectrometry for blood vessel detection during stereotactic biopsy of brain tumors', *Journal of Biophotonics* .

McCollough, C. et al. (2009), 'In defense of body CT', *AJR. American journal of roentgenology* **193**(1), 28.

McNitt-Gray et al. (2002), 'Aapm/rsna physics tutorial for residents: Topics in CT: Radiation dose in CT 1', *Radiographics* **22**(6), 1541–1553.

Medioni, G. & Kang, S. B. (2004), *Emerging topics in computer vision*, Prentice Hall PTR.

Mettler et al. (2000), 'CT scanning: patterns of use and dose', *Journal of radiological Protection* **20**(4), 353.

Mielke, R. et al. (2000), 'Navigation in knee endoprosthesis implantation–preliminary experiences and prospective comparative study with conventional implantation technique', *Zeitschrift fur Orthopadie und ihre Grenzgebiete* **139**(2), 109–116.

Moncharmont, L. et al. (2015), 'Phantom evaluation of a navigation system for out-of-plane CT-guided puncture', **96**.

Na, D. G. et al. (2012), 'Core-needle biopsy is more useful than repeat fine-needle aspiration in thyroid nodules read as nondiagnostic or atypia of undetermined significance by the bethesda system for reporting thyroid cytopathology', *Thyroid* **22**(5), 468–475.

Nakazawa, T. et al. (2014), 'Three-dimensional inline inspection for substrate warpage and ball grid array coplanarity using stereo vision', *Applied optics* **53**(14), 3101–3109.

Nicolau, S. et al. (2005), 'An augmented reality system to guide radio-frequency tumour ablation', *Computer animation and virtual worlds* .

Nie, S. et al. (2007), 'Nanotechnology applications in cancer', *Annu. Rev. Biomed. Eng.* **9**, 257–288.

OECD Health Data (2016), `https://data.oecd.org/healthcare/computed-tomography-ct-exams.htm`. Accessed: 2016-05-30.

Ogbole, G. (2010), 'Radiation dose in paediatric computed tomography: risks and benefits', *Annals of Ibadan postgraduate medicine* **8**(2), 118–126.

Oliva, A. et al. (2001), 'Modeling the shape of the scene: A holistic representation of the spatial envelope', *International journal of computer vision* **42**(3), 145–175.

Ozan, S. et al. (2014), 'Calibration of double stripe 3d laser scanner systems using planarity and orthogonality constraints', *Digital Signal Processing* **24**, 231–243.

Ozdemir, Z. M. et al. (2015), 'Image-guided percutaneous bone biopsy with a simulated van sonnenberg removable hub system', *The Eurasian journal of medicine* **47**(1), 1.

Pappa, V. et al. (1996), 'Role of image-guided core-needle biopsy in the management of patients with lymphoma.', *Journal of Clinical Oncology* **14**(9), 2427–2430.

Patient Positioning National Electrical Manufacturers Association (2016), `http://dicom.nema.org/`. Accessed: 2016-08-22.

Peters, T. M. (2001), 'Image-guided surgery: From x-rays to virtual reality', *Computer Methods in Biomechanics and Biomedical Engineering* **4**.

Phan, L. et al. (2015), 'Infrared invisibility stickers inspired by cephalopods', *Journal of Materials Chemistry C* .

Physics Central (2016), `http://www.physicscentral.com/`. Accessed: 2016-05-30.

Pitman, A. et al. (2009), 'The royal australian and new zealand college of radiologists (ranzcr) relative value unit workload model, its limitations and the evolution to a safety, quality and performance framework', *Journal of medical imaging and radiation oncology* **53**(5), 450–458.

Prochazka, A. et al. (2015), 'Bayesian classification and analysis of gait disorders using image and depth sensors of microsoft kinect', *Digital Signal Processing* .

Protection, A. R. et al. (2000), 'Australian radiation protection and nuclear safety agency'.

Sainani, N. et al. (2013), 'The challenging image-guided abdominal mass biopsy: established and emerging techniques if you can see it, you can biopsy it', *Abdominal imaging* **38**(4), 672–696.

Sannazzari, G. et al. (2002), 'CTMRI image fusion for delineation of volumes in three-dimensional conformal radiation therapy in the treatment of localized prostate cancer', *The British journal of radiology* **75**.

Schauer, D. et al. (2009), 'National council on radiation protection and measurements report shows substantial medical exposure increase 1', *Radiology* **253**(2), 293–296.

Schober, P. et al. (2011), 'Nirs (near-infrared spectroscopy) measurement of peripheral tissue oxygenation using the nonin equanox 7600 is not disturbed in helicopter-ems (hems) environment', *Medimond International Proceedings. Editografica, Bologna, Italy* .

Schubert, T. et al. (2013), 'CT-guided interventions using a free-hand, optical tracking system: initial clinical experience', *Cardiovascular and interventional radiology* **36**(4), 1055–1062.

Seeram, E. (2009), *Computed Tomography: Physical Principles, Clinical Applications, and Quality Control.*

Shar, B. et al. (2010), Towards three-dimensional fusion of infrared guidance measurements for biopsy procedures: some preliminary results and design considerations, *in* 'Signal Processing and Communication Systems (ICSPCS), 2010 4th International Conference on', IEEE, pp. 1–5.

Siemens Circa 1975 (n.d.), `http://www.healthcare.siemens.com/computed-tomography`. Accessed: 2016-05-30.

Sklair-Levy et al. (2000), 'CT-guided core-needle biopsy in the diagnosis of mediastinal lymphoma', *European radiology* **10**(5), 714–718.

Slovis, T. (2003), 'Children, computed tomography radiation dose, and the as low as reasonably achievable (alara) concept', *Pediatrics* **112**(4), 971–972.

Smith-Bindman, R. et al. (2008), 'Rising use of diagnostic medical imaging in a large integrated health system', *Health Affairs* **27**(6), 1491–1502.

Smith-Bindman, R. et al. (2009), 'Radiation dose associated with common computed tomography examinations and the associated lifetime attributable risk of cancer', *Archives of internal medicine* .

Sonka, M. et al. (2007), *Image Processing, Analysis, and Machine Vision*, Thomson-Engineering.

Stein, G. (1995), Accurate internal camera calibration using rotation, with analysis of sources of error, *in* 'Computer Vision, 1995. Proceedings., Fifth International Conference on', IEEE, pp. 230–236.

Taguchi, K. et al. (2000), 'High temporal resolution for multislice helical computed tomography', *Medical physics* **27**(5), 861–872.

Teeuwisse, W. et al. (2001), 'Patient and staff dose during CT guided biopsy, drainage and coagulation', *British Journal of Radiology* **74**.

Toporek, G. et al. (n.d.), 'Accuracy of navigated percutaneous needle insertions', *Nanophotonics* .

Toshiba Healthcare - CT Technology (2016), `http://www.toshiba-medical.eu/`. Accessed: 2016-10-11.

Tsiklakis, K. et al. (2014), 'Radiographic examination of the temporomandibular joint using cone beam computed tomography', *Dentomaxillofacial Radiology* .

UN (2008), *Report of the United Nations Scientific Committee on the Effects of Atomic Radiation: Fifty-sixth Session (10-18 July 2008).*, number 46, United Nations Publications.

Vahrmeijer, A. et al. (2013), 'Image-guided cancer surgery using near-infrared fluorescence', *Nature Reviews Clinical Oncology* **10**.

Varro, Z. et al. (2004), 'Laser navigation for radiofrequency ablation.', *CardioVascular and Interventional Radiology* **27**(5).

Wang, J. et al. (2013), 'Computational model of stereoscopic 3d visual saliency', *IEEE Transactions on Image Processing* **22**(6), 2151–2165.

Wang, Z. (2015), 'An imaging and measurement system for robust reconstruction of weld pool during arc welding', *Industrial Electronics, IEEE Transactions on* **62**(8), 5109–5118.

Webb, W. R. et al. (2014*a*), *Fundamentals of body CT*, Elsevier Health Sciences.

Webb, W. R. et al. (2014*b*), *Fundamentals of body CT*, Elsevier Health Sciences.

Weir, V. et al. (2014), 'Impact of physician practice on patient radiation dose during CT guided biopsy procedures', **22**(3).

Wood, B. J. et al. (2010), 'Navigation systems for ablation', *Journal of Vascular and Interventional Radiology* **21**(8), S257–S263.

Xu, G. et al. (2013), *Epipolar geometry in stereo, motion and object recognition: a unified approach*, Vol. 6, Springer Science & Business Media.

Yaniv, Z. et al. (2009), 'Electromagnetic tracking in the clinical environment', *Medical physics* **36**(3), 876–892.

Yu, L. et al. (2009), 'Radiation dose reduction in computed tomography: techniques and future perspective', *Imaging in medicine* **1**(1), 65–84.

Žabić, S. et al. (2013), 'A low dose simulation tool for CT systems with energy integrating detectors', *Medical physics* **40**(3), 031102.

Zaidi, H. et al. (2008), 'The clinical role of fusion imaging using PET, CT, and MR imaging', *PET Clinics* **3**.

Zhang, Z. (2000), 'A flexible new technique for camera calibration', *IEEE Transactions on pattern analysis and machine intelligence* **22**(11), 1330–1334.

Zoubir, A. (1997), The bootstrap: A tool for signal processing, *in* 'Signals, Systems & Computers, 1997. Conference Record of the Thirty-First Asilomar Conference on', Vol. 1, IEEE, pp. 433–437.

Appendix A

Results - Freehand Method v Infrared Guidance

Actual angle and outcome angles recorded in section 5.1.

Operator	Actual	Outcome	Diff	Operator	Actual	Outcome	Diff
Freehand	0	3	3	Infrared	0	0	0
Freehand	24	47.2	23.2	Infrared	24	21.4	2.6
Freehand	30	40.1	10.1	Infrared	30	28.5	1.5
Freehand	40	26.6	13.4	Infrared	40	36.1	3.9
Freehand	30	44.8	14.8	Infrared	30	27.3	2.7
Freehand	34	38.9	4.9	Infrared	34	28.4	5.6
Freehand	10	21.3	11.3	Infrared	10	10.7	0.7
Freehand	14	25.2	11.2	Infrared	14	12.2	1.8
Freehand	46	51.3	5.3	Infrared	46	41.5	4.5
Freehand	36	36.4	0.4	Infrared	36	34.7	1.3
Freehand	17	31.1	14.1	Infrared	17	18	1
Freehand	23	36.8	13.8	Infrared	23	20.3	2.7
Freehand	46	52	6	Infrared	46	42.3	3.7
Freehand	8	16.2	8.2	Infrared	8	7.2	0.8
Freehand	40	36.2	3.8	Infrared	40	36.7	3.3
Freehand	-1	-2	1	Infrared	-1	-4.7	3.7

Freehand	21	19.6	1.4	Infrared	21	16.4	4.6
Freehand	-29	-27.9	1.1	Infrared	-29	-28	1
Freehand	-41	-36.9	4.1	Infrared	-41	-38.4	2.6
Freehand	-30	-31.6	1.6	Infrared	-30	-28	2
Freehand	33	31.2	1.8	Infrared	33	29.6	3.4
Freehand	-9	-8.6	0.4	Infrared	-9	-11.7	2.7
Freehand	15	16.2	1.2	Infrared	15	11.1	3.9
Freehand	-45	-43.5	1.5	Infrared	-45	-44.4	0.6
Freehand	-36	-38.3	2.3	Infrared	-36	-33.9	2.1
Freehand	-16	-16.4	0.4	Infrared	-16	-16.5	0.5
Freehand	23	17.4	5.6	Infrared	23	17.6	5.4
Freehand	-45	-46.6	1.6	Infrared	-45	-36.9	8.1
Freehand	9	6.2	2.8	Infrared	9	6.2	2.8
Freehand	41	41.8	0.8	Infrared	41	30.5	10.5

Appendix B

Results - Infrared to DICOM

The raw (u, v) coordinates returned by each of the the Wii Remotes and the corresponding (x, y) mapping of the (u, v) data for the two IR sources. These results refer back to section 5.1.

U_1	V_1	U_2	V_2	X	Y
247	243	473	244	1084	528
209	244	439	251	943	533
220	133	461	144	966	526
245	244	479	251	1109	529
224	133	486	140	903	525
199	126	411	134	785	527
113	125	364	139	632	531
89	134	323	140	447	535
50	126	346	145	355	544
160	130	407	141	651	539
98	234	358	239	441	536
21	126	281	133	267	540
3	137	229	142	152	545
1	137	217	145	90	550
43	244	270	252	275	555
188	120	412	125	873	525

91	120	364	126	682	530
82	117	345	123	523	528
24	117	293	133	325	534
1	1	218	140	57	544

Appendix C

2D to 3D Transformation Results

The system was tested with real data from the two IR sensors where real-time data acquisition was able to translate to the estimated 3D position as the IR sources are moved. These results refer back to section 5.2.

3D Experimental Results					
	U_1, V_1	U_2, V_2	Actual X,Y,Z	Predicted X,Y,Z	Error
1	-17 -327	-181 -312	3 3 8	2.97 3.05 7.98	0.059488
2	-128 -103	-217 -105	3 11 12	2.92 11.02 11.92	0.114629
3	-153 -341	-223 -382	3 3 13	3.12 3 13.10	0.151855
4	-157 -243	-254 -280	2 6 13	1.99 5.96 12.95	0.068123
5	-136 -471	-27 -436	10 2 14	10.09 2 13.97	0.089067
6	195 -130	14 -30	9 11 2	9.12 11.04 1.97	0.12799
7	77 -220	-105 -165	5 7 5	5.11 7.07 5.02	0.131698
8	-77 -403	-127 -391	6 2 11	5.82 1.90 10.98	0.206607
9	75 -80	-179 -35	2 11 4	1.98 11.07 4.05	0.092121
10	-191 -382	-287 -455	1 1 14	1.16 1.03 14.06	0.173583
11	194 -407	55 -275	11 3 3	10.85 2.84 2.91	0.235548
12	-82 -283	-250 -305	1 4 10	1.10 3.99 9.95	0.10737
13	-38 -306	16 -237	11 7 11	11 6.98 10.95	0.053596
14	-122 -468	29 -406	12 3 14	12.02 2.98 13.94	0.062632
15	-60 -82	-246 -76	1 11 9	0.94 11 8.95	0.074252

16	-27 -353	-135 -330	5 3 9	4.98 2.97 8.94	0.073299
17	51 -194	-186 -162	2 7 5	1.94 6.99 4.98	0.06271
18	31 -445	57 -340	12 3 9	12.07 3.04 9.04	0.091185
19	198 -252	129 -111	14 9 4	14.05 9.04 4.11	0.12444
20	-143 -505	83 -423	14 3 15	14.06 3.03 15.03	0.07663
21	6 -64	-177 -31	3 12 7	2.95 12.04 6.99	0.068387
22	297 -87	164 52	15 14 1	15.04 14 1.07	0.078823
23	-156 -45	-227 -51	3 13 13	2.96 13.01 12.94	0.074921
24	19 -355	-217 -350	1 1 6	1.03 0.99 6.03	0.042534
25	13 -417	5 -341	10 3 9	10.16 2.96 9.05	0.169506
26	-1 -409	-124 -380	5 1 8	5.13 1.02 8.05	0.141825
27	171 -344	-106 -270	4 2 1	3.94 1.96 0.96	0.085204
28	19 -299	-217 -290	1 3 6	1.04 3 6.01	0.04375
29	244 -54	67 56	11 14 1	11.18 14 1	0.181548
30	30 -27	-94 22	6 14 7	5.99 13.97 6.98	0.039591
31	110 -227	-145 -174	3 6 3	2.96 5.99 3	0.042082
32	-138 -202	-275 -232	1 7 12	0.86 6.98 11.95	0.147878
33	-116 -28	-163 -11	5 14 12	5 14.04 11.73	0.269662
34	66 -46	-206 -7	1 12 4	0.94 11.97 3.98	0.071273
35	-188 -368	-124 -380	7 4 15	7.06 3.99 15.04	0.071378
36	146 -348	-111 -280	4 2 2	4.01 1.98 2	0.023806
37	-173 -62	-179 -63	5 13 14	4.91 13 13.89	0.138336
38	41 -187	-65 -131	7 9 7	7.17 8.96 7.03	0.177943
39	141 -258	120 -130	14 9 6	13.97 8.97 5.97	0.053351
40	-131 -139	-111 -123	7 11 13	7.02 11.01 13.01	0.029379
41	164 -251	55 -134	11 8 4	11.15 8.10 4.12	0.21589
42	57 -4	-163 40	3 14 5	2.73 13.94 4.91	0.29371
43	268 -89	159 46	15 14 2	14.96 14.04 2.21	0.217884
44	68 -184	-134 -135	4 8 5	3.96 8 4.99	0.041195
45	196 -224	14 -115	9 8 2	9.11 8.06 2.09	0.15943
46	-92 -228	-175 -224	4 7 11	4.15 7.08 11.02	0.171905
47	50 -372	109 -250	14 6 9	14.02 6.02 9.02	0.030635
48	126 -306	25 -200	10 6 5	10.14 6.11 5.09	0.197206

49	-47 -359	-12 -308	10 5 11	9.99 4.83 11.02	0.176149
50	199 -185	129 -52	14 11 4	14.08 11.07 4.10	0.150158
51	-72 -175	11 -120	11 11 12	11.09 11.01 12.04	0.097547
52	-94 -326	30 -260	12 7 13	11.91 7 12.97	0.098489
53	-31 -284	41 -205	12 8 11	11.91 8.02 10.96	0.098073
54	-214 -397	-269 -470	2 1 15	2.10 1.05 15.05	0.125974
55	260 -478	134 -290	14 2 2	13.87 2.06 2.03	0.140123
56	121 -322	-119 -260	4 3 3	3.95 3.01 2.98	0.054411
57	-21 -395	-116 -361	6 2 9	5.64 1.94 8.91	0.374986
58	-62 31	-248 41	1 15 9	0.31 14.82 8.80	0.744389
59	173 -35	76 63	12 15 4	12.12 15 4.01	0.120867
60	-166 -118	-284 -145	1 10 13	0.89 10 12.92	0.132711
61	-195 25	-295 6	1 15 14	0.67 14.93 14.01	0.335898
62	-29 -522	47 -430	12 1 11	12.06 1 11.03	0.064268
63	229 -315	135 -160	14 7 3	14.09 7.03 3.05	0.109068
64	-87 -56	-154 -34	5 13 11	4.91 13.06 10.83	0.20326
65	-108 -159	-135 -144	6 10 12	5.87 9.97 11.96	0.135162
66	-100 -159	-208 -161	3 9 11	3 9.02 11.02	0.02815
67	90 -44	-197 4	1 12 3	1.48 12.22 3.36	0.639195
68	103 -190	-108 -132	5 8 4	4.70 7.82 3.83	0.386079
69	-93 -273	-72 -245	8 7 12	8.12 7.01 12.05	0.134136
70	191 -338	-58 -244	6 3 1	5.90 2.97 0.98	0.106867
71	28 -284	131 -170	15 9 10	15 8.98 9.99	0.024837
72	-24 -341	-204 -345	2 2 8	2.20 2.08 8.06	0.227596
73	77 -251	-107 -194	5 6 5	5 6.05 5.02	0.056716
74	-23 -228	75 -143	13 10 11	13.17 10.07 11.03	0.18497
75	160 -307	-14 -210	8 5 3	8.16 5.02 3.03	0.169135
76	-56 -300	65 -225	13 8 12	12.95 7.89 12.07	0.135895
77	171 -175	-105 -101	4 8 1	4.03 7.97 0.92	0.092385
78	74 -220	-174 -182	2 6 4	2.16 6.05 4.14	0.217755
79	32 -445	53 -340	12 3 9	11.91 2.98 8.96	0.098296
80	-25 -279	-35 -223	9 7 10	8.93 6.97 9.93	0.099611
81	-184 -98	-264 -125	2 11 14	2 10.99 13.89	0.114311

82	-103 17	-209 26	3 15 11	2.66 14.93 10.99	0.347023
83	137 -109	-75 -33	6 11 3	5.81 11.07 3.10	0.227023
84	-147 -226	-61 -201	9 9 14	8.98 9.02 13.98	0.037088
85	57 -49	-19 15	9 14 7	8.88 13.82 6.80	0.293268
86	-1 -84	-200 -60	2 11 7	2.09 11.05 7.01	0.102926
87	256 -175	137 -35	14 11 2	14.05 11.10 1.98	0.111041
88	-198 -435	-185 -475	5 1 15	4.93 1.01 14.99	0.066702
89	138 -167	-65 -90	6 9 3	6.19 9.10 3.08	0.228191
90	255 -110	130 15	14 13 2	13.61 12.59 1.01	1.140771
91	-32 -213	40 -143	12 10 11	11.89 10.01 10.97	0.112861
92	-93 -425	30 -360	12 4 13	11.87 4 13	0.128695
93	-37 -254	120 -156	15 10 12	14.93 10.03 11.96	0.082942
94	110 -191	117 -76	14 11 7	14.06 11.08 7.02	0.098969
95	-132 -144	-5 -106	11 12 14	10.94 12.01 13.94	0.082015
96	92 -501	67 -374	12 1 7	12.05 1.10 7.02	0.115538
97	87 -320	-83 -253	6 4 5	5.90 4.06 4.99	0.118894
98	108 -90	117 11	14 14 7	14.06 13.96 6.95	0.088236
99	-103 -370	110 -279	15 7 14	14.85 6.96 13.97	0.152527
100	-4 -454	-55 -395	8 1 9	7.91 0.99 8.98	0.092522

Appendix D

Training Module

Training module comprising of a biopsy needle with an infrared reflective tape on its hub, an infrared illuminator and detector as well as a laptop computer.

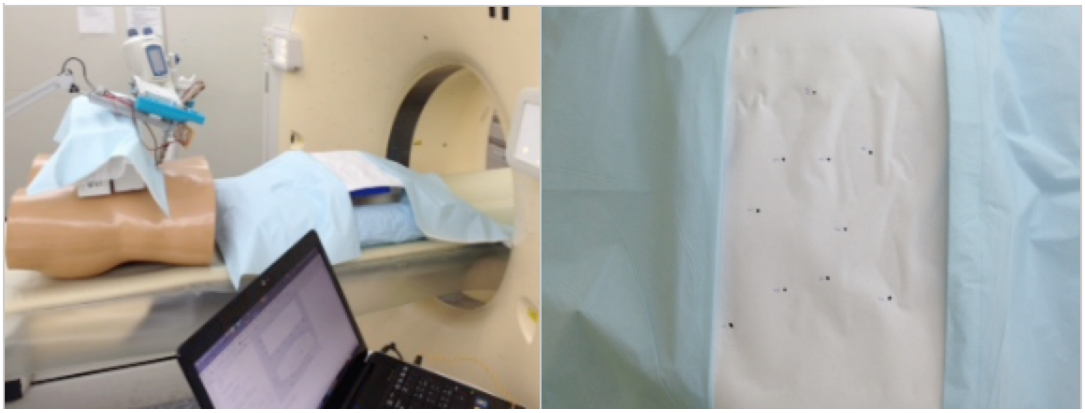

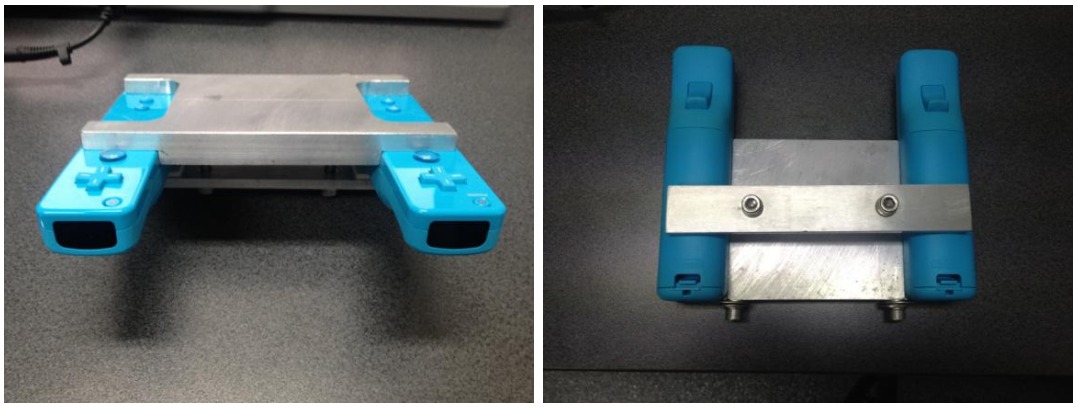

Appendix E

Connect Client to Drivers, Read and Run the Program

The 'wiiuse - The Wiimote C Library' was used as the drivers for the system. These drivers are registered to /dev/wiimote, where the device is read from using MATLAB code.

1. Load wiimote drivers to kernel
2. Connect from client application to drivers
3. Request data from wiimote
4. Process and plot data from wiimote
5. Repeat steps 3 and 4 until the client program is closed

```
function [ wii ] = infranav()
    [ status ] = wii2mat( wii.start );

    M = 10;
    coord.pitch = zeros(2,M);
    coord.roll = zeros(2,M);
    coord.yaw = zeros(2,M);
```

```
    coord.ir.x = zeros(2,M);
    coord.ir.y = zeros(2,M);
    coord.ir.z = zeros(2,M);

    hfig = figure('Name','WiiPlot','Position',[700 300 560 420],
    'PaperPositionMode','auto');

    while( ishandle(hfig))
        [ wii ] = wii2mat( wii.read );

        coord.pitch(:,1:end-1) = coord.pitch(:,2:end);
        coord.roll(:,1:end-1)  = coord.roll(:,2:end);
        coord.yaw(:,1:end-1)   = coord.yaw(:,2:end);
        coord.ir.x(:,1:end-1)  = coord.ir.x(:,2:end);
        coord.ir.y(:,1:end-1)  = coord.ir.y(:,2:end);
        coord.ir.z(:,1:end-1)  = coord.ir.z(:,2:end);

        coord.pitch(:,end) = wii.data.pitch;
        coord.roll(:,end)  = wii.data.roll;
        coord.yaw(:,end)   = wii.data.yaw;
        coord.ir.x(:,end)  = wii.data.ir.x;
        coord.ir.y(:,end)  = wii.data.ir.y;
        coord.ir.z(:,end)  = wii.data.ir.z;

        plot( coord.ir.x(1,:), coord.ir.y(1,:), 'rx' ); hold on;
        plot( coord.ir.x(2,:), coord.ir.y(2,:), 'bo' ); hold off;

        pause(0.01)
    end
```

```
function [ output ] = wii2mat( varargin )

    wii = struct( 'start',0, 'init',1,'find',2,'connect',
    3,'rumble',4,'status',5,'read',6,'write',7,'is_connected',
    8,'disconnect',9,'stop',10 );

        switch( size(varargin,2)==1 )
```

```
case 1

    switch( class( varargin{1}) )

    case 'char'
        action= varargin{1};

    case 'double'
        action='wii2mat';
        command=varargin{1};

    otherwise
        error('');

    end

otherwise
    error('');

end
switch( action )

case 'init'
    output = wii;
    return;
case 'wii2mat'
    response = w2m( num2str(command) );

    switch( command )

    case wii.start
        output = response;

    case wii.init
        output = response;
```

```
        case wii.find
            output = response;

        case wii.connect
            output = response;

        case wii.rumble
            output = response;

        case wii.status
            output = response;

        case wii.read
            response = str2num( response );
            response( response==0 ) = -1;
            response = reshape( response, 6, 2 ).';

            output = wii;
            output.data.pitch = response(:,1);
            output.data.roll  = response(:,2);
            output.data.yaw   = response(:,3);
            output.data.ir.x  = response(:,4);
            output.data.ir.y  = response(:,5);
            output.data.ir.z  = response(:,6);

        case wii.write
            output = response;
        case wii.is_connected
            output = logical( str2num(response) );
        case wii.disconnect
            output = response;
        case wii.stop
            output = response;
        otherwise
            error('');
        end
    otherwise
```

```
        error('');
    end
```

```
#include <sys/types.h>
#include <sys/stat.h>
#include <stdio.h>
#include <stdlib.h>
#include <fcntl.h>
#include <errno.h>
#include <unistd.h>
#include <string.h>
#include <assert.h>
#include <signal.h>
#include <ctype.h>
#include <wait.h>

#include <vector>
#include <algorithm>

#ifndef WIN32
        #include <unistd.h>
#endif

#include "wiiuse.h"
#include "w2m.hpp"

#ifdef MEX
#include "matrix.h"
#include "mex.h"
#endif


using namespace std;

#include "fullduplex.hpp"
```

```
#ifndef MEX
int main(int argc, char** argv) {
#else
void mexFunction(int nlhs, mxArray *plhs[], int nrhs, const mxArray
*prhs[]) {
#endif

    char *input_buf;
    int   buflen, status;
    int wrfd, rdfd, numread, numwrite;
    char rdbuf[MAX_BUFFER_SIZE];
    double *x,*y;

    if (nrhs != 1) mexErrMsgTxt("One input required.");
    else if (nlhs > 1) mexErrMsgTxt("Too many output arguments.");
if (mxIsChar(prhs[0]) != 1) mexErrMsgTxt("Input must be a string.");
if (mxGetM(prhs[0]) != 1) mexErrMsgTxt("Input must be a row vector.");
if (mxGetN(prhs[0]) != 1) mexErrMsgTxt("Input must be a col vector.");


    /* Get the length of the input string. */
    buflen = (mxGetM(prhs[0]) * mxGetN(prhs[0])) + 1;

    /* Allocate memory for input and output strings. */
    input_buf = (char*)mxCalloc(buflen, sizeof(char));

    /* Copy the string data from prhs[0] into a C string input_buf. */
    status = mxGetString(prhs[0], input_buf, buflen);
    if (status!=0) mexWarnMsgTxt
    ("Not enough space. String is truncated.");

    /* Open the first named pipe for writing */
    wrfd = open(NAMED_PIPE_TO_WIIMOTE, O_WRONLY);

    /* Open the second named pipe for reading */
    rdfd = open(NAMED_PIPE_FROM_WIIMOTE, O_RDONLY);
```

```
    /* Write to the pipe */
    //numwrite = write(wrfd, argv[1], strlen(argv[1]));
    numwrite = write(wrfd, input_buf, buflen);



    /* Read from the pipe */
    numread = read(rdfd, rdbuf, MAX_BUFFER_SIZE);
    rdbuf[numread] = '\0';

    printf("Full Duplex Client : Read From the Pipe : s\n", rdbuf);

    plhs[0] = mxCreateString( rdbuf );

    close(rdfd);
    close(wrfd);

    #ifndef MEX
        return 0;
    #else
                return;
    #endif
}
```

Appendix F

Ethical Clearance

Dr Mark Benson
Director & Chair
Radiology Department
Princess Alexandra Hospital
Ipswich Road
Woolloongabba, QLD 4102

Re: Permission to access data and carry out research in the radiology department.

Dear Dr Benson,

I have previously discussed with you undertaking a project that is relevant to my duties within PACS/RIS support. I'm seeking your support and assistance to complete this work.

The study will involve the use of large radiology datasets (images) and some after hours use of our CT scanner. I am seeking permission to use selected large datasets from the PACS archive as test objects. All datasets will be appropriately de-identified prior to use.

I believe that the research will be mutually beneficial for the hospital, the University and myself. The expected outcomes of the research are detailed in the attached summary of the research. I am also seeking your general support and assistance with access to the PACS technologies and your input as an unofficial local supervisor to this work.

At the completion of the project I hope to develop publications in a relevant journal from the work.

Thank you for your time.
Yours sincerely,
Bruce Shar - 23rd May 2009

Permission to access data and carry out research in the radiology department was granted

Appendix G

Radiologist Survey Questions

The navigation system ...	−−	−	−/+	+	++	**The navigation system ...**
is complicated to use	☐	☐	☐	☐	☐	is easy to use
does not help with spatial referencing	☐	☐	☐	☐	☐	helps with spatial referencing
is not useful for the purposes of education	☐	☐	☐	☐	☐	is useful for the purposes of education
is slow and not very robust	☐	☐	☐	☐	☐	is fast and robust
doesn't detect the needle properly	☐	☐	☐	☐	☐	detects the needle effectively
the needle cannot easily be sterilised	☐	☐	☐	☐	☐	the needle can easily be sterilised
the infrared tape has a negative impact on the trajectory	☐	☐	☐	☐	☐	the infrared tape has no negative impact on the trajectory
the system doesn't help reduce the number of required scans	☐	☐	☐	☐	☐	the system helps reduce the number of required scans
is disruptive during the biopsy procedure	☐	☐	☐	☐	☐	is not disruptive during the biopsy procedure
The graphical user interface is too simple	☐	☐	☐	☐	☐	the graphical user interfaces simplicity is an advantage
integrating this navigation system with the CT scanner is unnecessary	☐	☐	☐	☐	☐	integrating this navigation system with the CT scanner would be most helpful
i would not like to see this system tested in real biopsy scenarios	☐	☐	☐	☐	☐	i would like to see this system tested in real biopsy scenarios
if implemented this system would not save time during a biopsy procedure	☐	☐	☐	☐	☐	if implemented this system would definitely save time during a biopsy procedure

Appendix H

Radiologist Survey Results

Survey conducted by 45 Radiologists and clinicians who tested the Infrared Navigation System at the Princess Alexandra Hospital, Brisbane, Australia.

Marks	Q1	Q2	Q3	Q4	Q5	Q6	Q7	Q8	Q9	Q10	Q11	Q12	Q13
Excellent	29	36	35	30	17	43	32	38	36	38	42	41	42
Very Good	15	8	5	3	6	2	3	4	5	1	2	3	1
Good	1	1	2	5	13	0	5	0	4	4	1	0	1
Fair	0	0	2	4	8	0	5	1	0	1	0	1	1
Poor	0	0	1	3	1	0	0	2	0	1	0	0	0

Figure H.1: Survey Results - 45 Radiologists who operated the system and participated in the survey